Supporting information for

Multistep screening of transition metal based homonuclear double atom catalysts to unravel the electronic origin of their activity and selectivity challenges for nitrogen reduction.

Anjumun Rasool [a] and Manzoor Ahmad Dar[a]*

[a] Department of Chemistry, Islamic University of Science and Technology,

Awantipora, Jammu and Kashmir-192122, India

Table of contents

9. **Fig. S8.** Free energy profile for NRR on Nb_2 and La_2 DACs along the enzymatic mechanism
10. **Fig. S9.** Free energy profile for NRR on Hf_2 and Ta_2 DACs along alternating, distal and enzymatic mechanisms
11. **Fig. S10.** Free energy profile for NRR on W_2 DAC along distal and enzymatic mechanisms and on Re_2 DAC along alternate and distal mechanisms
12. **Fig. S11.** Optimized truncated side views of NRR intermediates on (a) V_2 and (b) Fe_2 DACs along alternating and distal mechanisms. Pink and green coloured arrows indicate alternating and distal mechanisms respectively
13. **Fig. S12.** Optimized truncated side views of NRR intermediates on Co_2 DAC along alternating, distal, and enzymatic mechanisms. Pink, green, and purple-coloured arrows indicate alternating, distal, and enzymatic mechanisms respectively
14. **Fig. S13.** Optimized truncated side views of NRR intermediates on Ni_2 DAC along alternating and distal mechanisms. Pink and green coloured arrows indicate alternating and distal mechanisms respectively
15. **Fig. S14.** Optimized truncated side views of NRR intermediates on (a) Nb_2 and (b) La_2 DACs along enzymatic mechanisms
16. **Fig. S15.** Optimized truncated side views of NRR intermediates on (a) Hf_2 (b) Ta_2 and (c) W_2 DACs along alternating, distal, and enzymatic mechanisms. Pink, green, and purple-coloured arrows indicate alternating, distal, and enzymatic mechanisms respectively.
17. **Fig. S16.** Optimized truncated side views of NRR intermediates on Re_2 DAC along alternating and distal mechanisms. Pink and green coloured arrows indicate alternating and distal mechanisms respectively.
18. **Fig. S17.** Free energy changes for adsorption of the NRR intermediates ($*N_2$, $*N_2H$, $*N_2H_2$, $*N_2H_3$, $*N_2H_4$, $*NH_2$ and $*NH_3$) on the screened DACs: plotted as a function of total transition metal dimer d- states near Fermi level (-3.0 to 3.0 eV). The data points from left to right are for La_2, Nb_2, Hf_2, Ta_2, V_2, W_2, Re_2, Fe_2, Ni_2 and Co_2 catalysts respectively. Solid lines are the fitted linear relation between free energies and total d-states of the intermediates, with the slope and intercept shown in the plot.
19. **Fig. S18**. The correlations between (a) adsorption energies of N_2 (ΔE_{*N_2}) and NNH (ΔE_{*NNH}), (b) adsorption energies of NH_2 (ΔE_{*NH_2}) and NH_3 (ΔE_{*NH_3}) intermediates adsorbed on screened out DACs.

20. **Fig. S19.** The scaling relationships for free energy of (a) $*N_2H$ vs $*N_2$, (b)* N_2H_2 vs $*N_2$, (c) $*N_2H_3$ vs $*N_2$, (d) $*N_2H_4$ vs $*N_2$, (e) $*NH_2$ vs $*N_2$, and (f) $*NH_3$ vs *N (NRR intermediates on the screened DACs).
21. **Fig. S20.** The projected density of states (PDOS) of (i) 3d, (ii) 4d, and (iii) 5d transition metal-based DACs. The PDOS of the total, TM-d, N-2p, C-2p and H-1s is plotted in grey, pink, dark green, blue and cyan colours, respectively.
22. **Fig. S21.** Computed crystal orbital Hamilton populations (COHPs) and respective orbital projected density of states (oPDOS) for the direct interaction between M_2–N bonds of the N_2 adsorbed on the screened DACs. The bonding and antibonding states in COHP are depicted by blue and red, respectively. Plots representing the correlation between (a) the calculated integrated crystal Hamilton population (ICOHP) of the bond between screened DACs and N atom/atoms of adsorbed $*N_2$ molecule and N-N bond length. (b) the calculated ICOHP of the bond between screened DACs and N atom/atoms of adsorbed $*N_2$ molecule and free energy change for $*N_2$ adsorption (ΔG_{*N_2}) (c) the calculated ICOHP of N-N bond on screened DACs and N-N bond length
23. **Fig. S22**. The crystal orbital Hamilton population (COHP) of N–N bond of N_2 on the screened DACs. The bonding and antibonding states in COHP are depicted by blue and red, respectively.
24. **Table S2.** Energy, ZPE, TS, G and ΔG of reaction steps of NRR on V_2, Fe_2 and Ni_2 DACs along alternating and distal mechanisms
25. **Table S3.** Energy, ZPE, TS, G and ΔG of reaction steps of NRR on Co_2 DAC along alternating, distal and enzymatic mechanisms
26. **Table S4.** Energy, ZPE, TS, G and ΔG of reaction steps of NRR on Nb_2 and La_2 DACs along the enzymatic mechanism
27. **Table S5.** Energy, ZPE, TS, G and ΔG of reaction steps of NRR on Hf_2, Ta_2 and W_2 DACs along alternating, distal and enzymatic mechanisms
28. **Table S6.** Energy, ZPE, TS, G and ΔG of reaction steps of NRR on Re_2 DAC along alternating and distal mechanisms

Table S1: Lattice parameters of the optimized unit cells of 3d, 4d and 5d transition metal-based DACs on TCNQ monolayer.

System	Lattice parameters
Sc_2@TCNQ	a=6.30 Å b=12.31 Å c=4.47 Å α= 114.47° β=45.65° γ=93.04°
Ti_2@TCNQ	a=8.44 Å b=11.37Å c=13.49 Å α=89.83° β=90.22° γ=89.86°
V_2@TCNQ	a=8.21 Å b=11.32 Å c=15.11 Å α=89.88° β=90.00° γ=89.64°
Cr_2@TCNQ	a=8.09 Å b=11.38 Å c=6.41 Å α=88.89° β=89.91° γ=89.88°
Mn_2@TCNQ	a=7.89 Å b=12.67 Å c=13.90 Å α=91.35° β=90.18° γ=89.95°
Fe_2@TCNQ	a=8.13 Å b=11.28 Å c=13.65 Å α=90.24° β=90.23° γ=89.58°
Co_2@TCNQ	a=8.04 Å b=10.97 Å c=13.35 Å α=89.13° β=90.22° γ=90.00°
Ni_2@TCNQ	a=8.07 Å b=11.12 Å c=15.01 Å α=90.99° β=89.80° γ=89.90°
Cu_2@TCNQ	a=8.13 Å b=11.34 Å c=13.14 Å α=90.24° β=89.25° c=94.47°
Y_2@TCNQ	a=8.60 Å b=11.72 Å c=6.94 Å α=89.80° β= 90.58° γ=89.87°
Zr_2@TCNQ	a=8.60 Å b=11.72 Å c=6.94 Å α=89.80° β= 90.58° γ=89.87°
Nb_2@TCNQ	a= 8.62 Å b= 11.31 Å c= 14.70 Å α= 90.57° β= 90.14° γ=89.77°

Tc_2@TCNQ	a= 7.93 Å b= 11.49 Å c= 4.18 Å α= 62.11° β= 119.87 ° γ= 88.58°
Mo_2@TCNQ	a= 8.47 Å b= 11.57 Å c= 14.77 Å α= 89.72° β= 90.07° γ= 89.57°
Ru_2@TCNQ	a=8.60 Å b=11.72 Å c=6.94 Å α=89.80° β= 90.58° γ=89.87°
Rh_2@TCNQ	a= 8.41 Å b= 10.96 Å c= 5.93 Å α= 87.64° β= 89.15° γ= 89.97°
Pd_2@TCNQ	a= 7.99 Å b= 10.74 Å c= 4.55 Å α= 53.98° β= 118.09° γ= 87.09°
Ag_2@TCNQ	a=8.60 Å b=11.72 Å c=6.94 Å α=89.80° β= 90.58° γ=89.87°
La_2@TCNQ	a=7.52 Å b=10.97 Å c=4.14 Å α=71.07° β=132.08° γ=115.92°
Hf_2@TCNQ	a=7.44 Å b=13.04 Å c=4.14 Å α=117.40° β=114.11° γ=92.75°
Ta_2@TCNQ	a=7.76 Å b=12.10 Å c=4.10 Å α=63.63° β= 116.91° γ=90.02°
W_2@TCNQ	a=7.65 Å b=10.28 Å c=4.15 Å α=82.22° β= 135.48° γ=96.21°
Re_2@TCNQ	a=7.73 Å b=10.47 Å c=3.85 Å α=69.92° β=47.79° γ=84.21°
Os_2@TCNQ	a=8.03 Å b=10.16 Å c=3.92 Å α=80.58° β=45.15° γ= 90.32°
Ir_2@TCNQ	a=8.41 Å b=10.87 Å c=5.04 Å α=88.30° β= 90.22° γ=90.22°
Pt_2@TCNQ	a=8.44 Å b=10.47 Å c=4.25 Å α=69.69° β=48.19° γ=88.42°

Au_2@TCNQ	a=8.54 Å	b=11.70 Å	c=5.98 Å
	α=90.91°	β= 91.08°	γ=89.78°

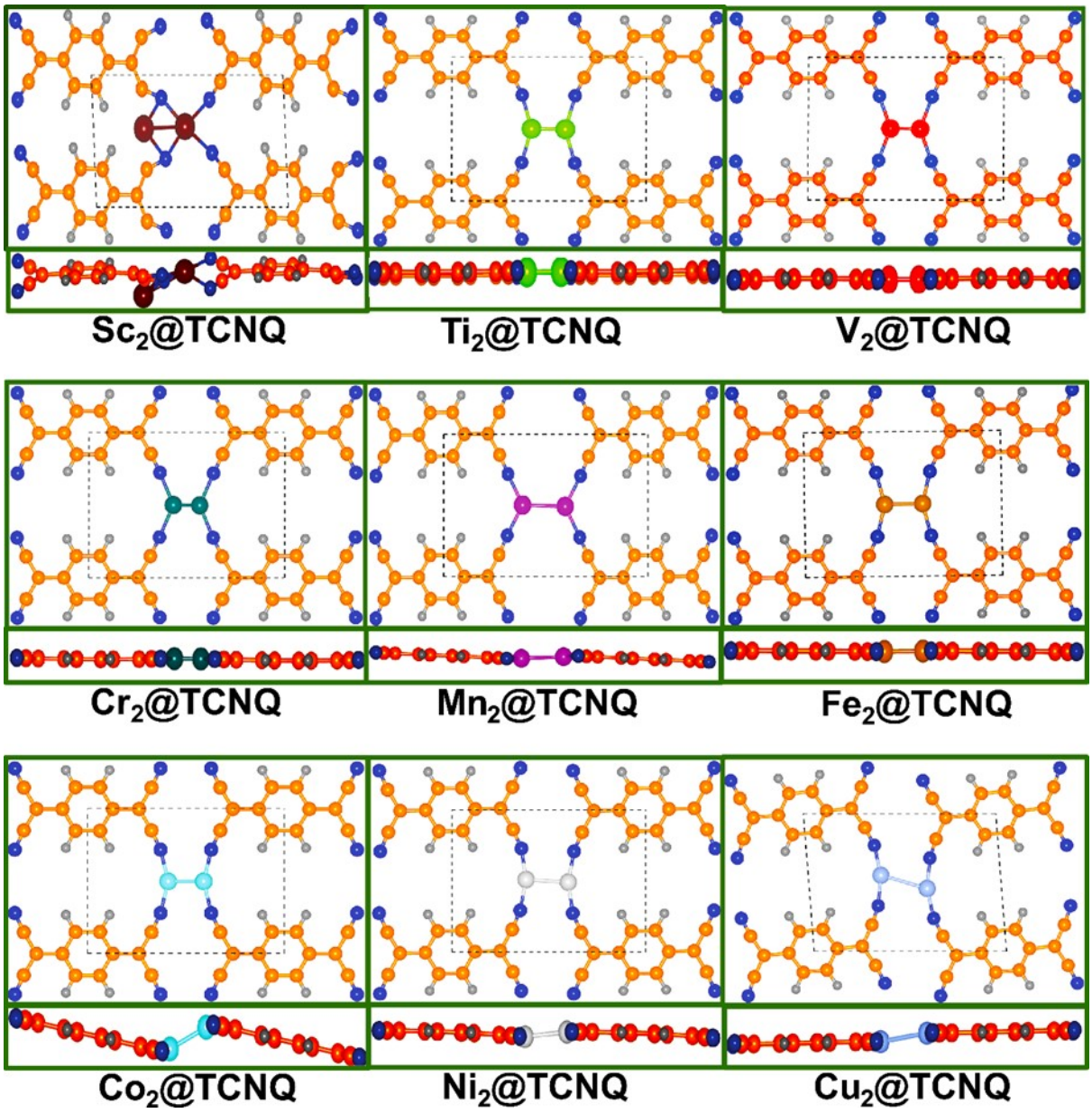

(a)

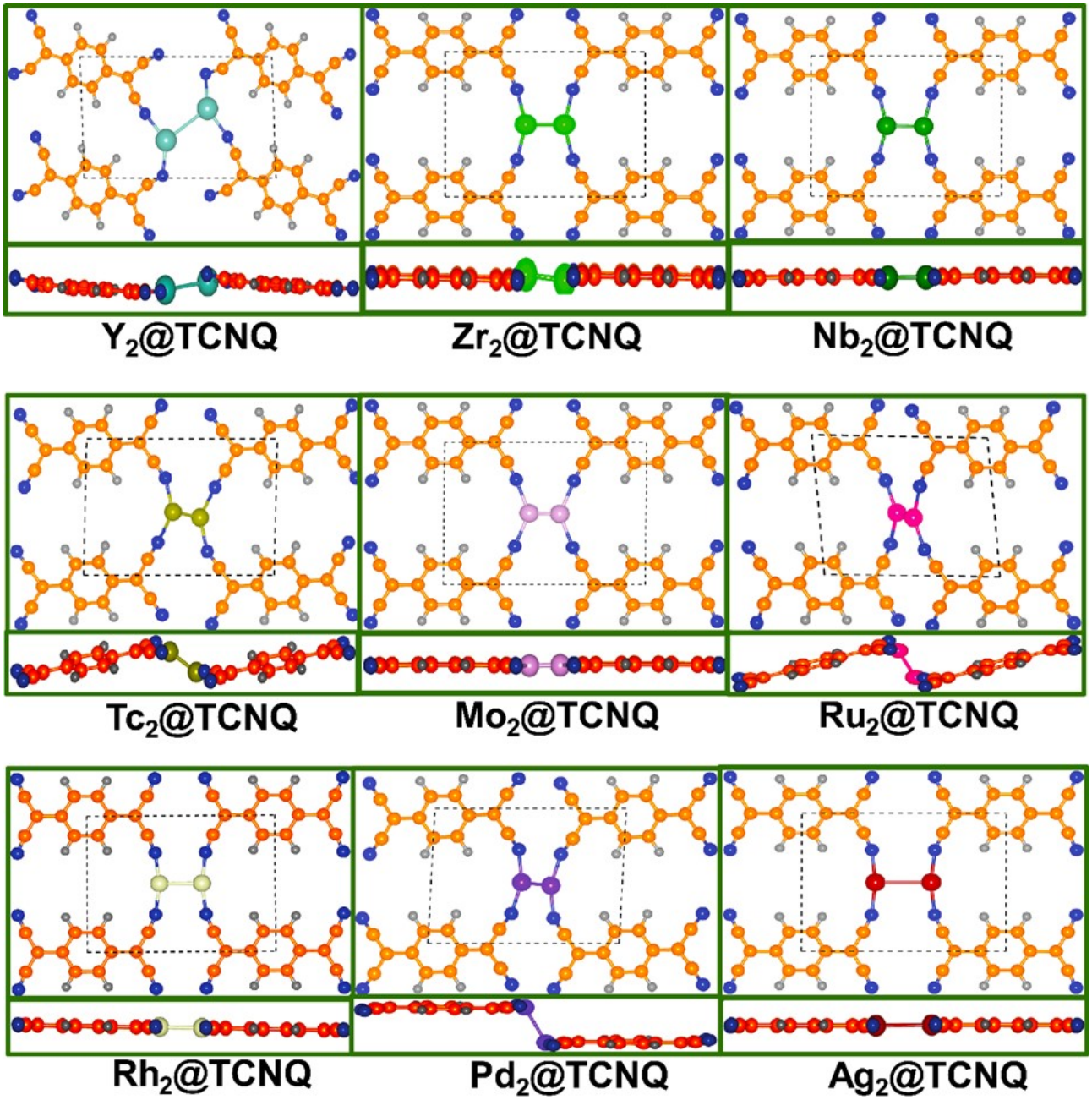
Y2@TCNQ
Zr2@TCNQ
Nb2@TCNQ
Tc2@TCNQ
Mo2@TCNQ
Ru2@TCNQ
Rh2@TCNQ
Pd2@TCNQ
Ag2@TCNQ

(b)

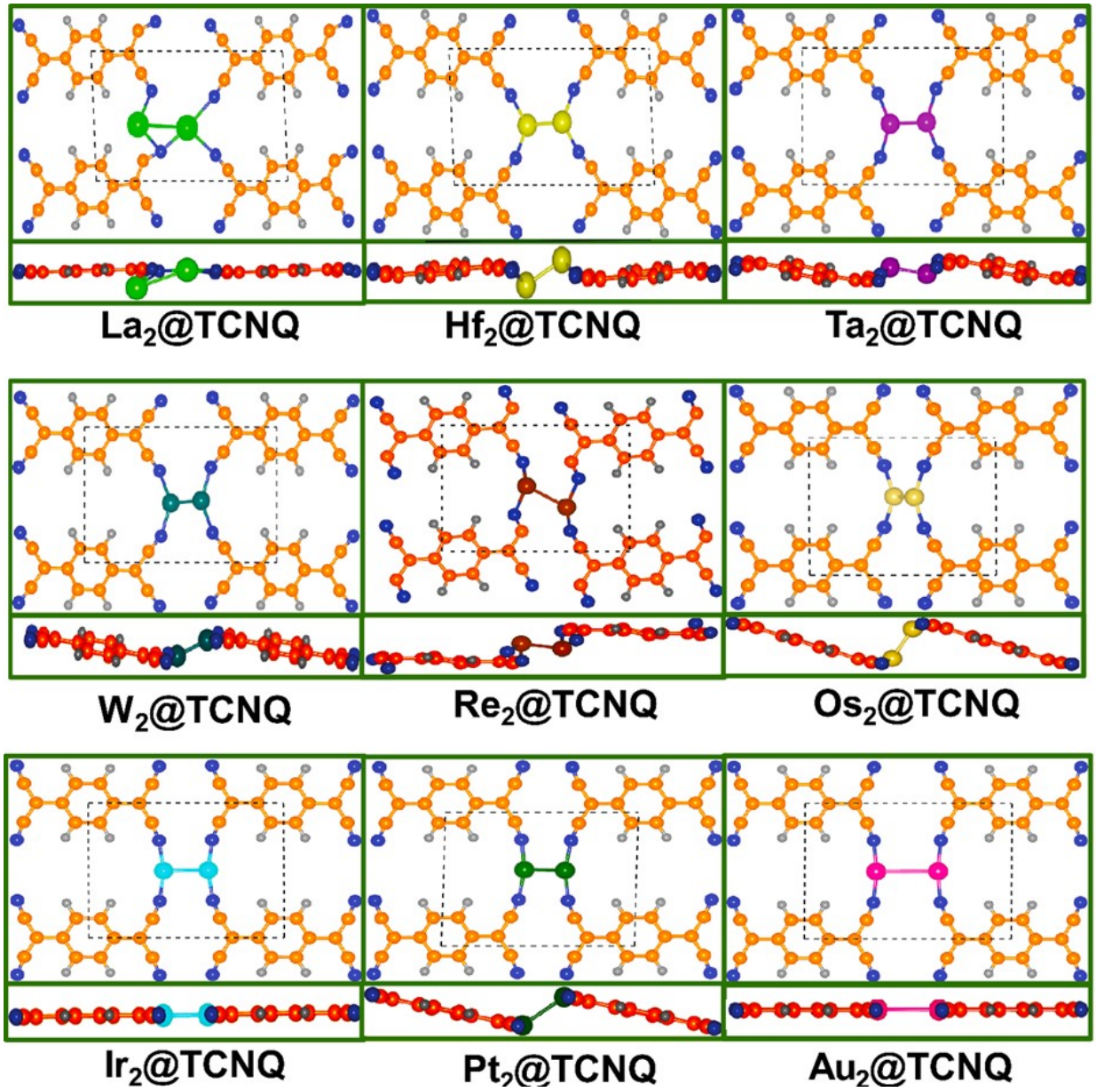

(c)

Fig. S1. Top and side views of the optimised structures of (a) 3d, (b) 4d, and (c) 5d transition metal-based DACs supported on TCNQ monolayer with binding energy values.

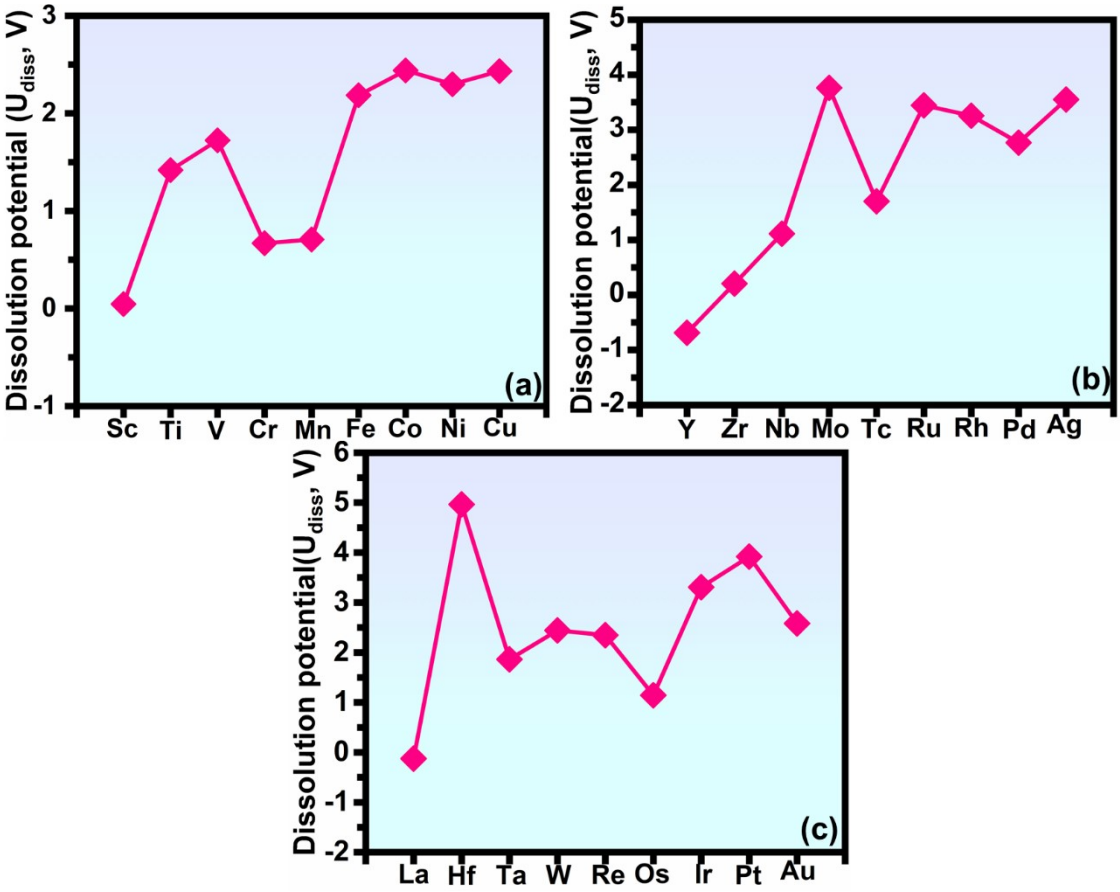

Fig. S2. Computed dissolution potential (U_{diss}) of (a)3d, (b) 4d and (c) 5d transition metal-based DACs supported on the TCNQ monolayer

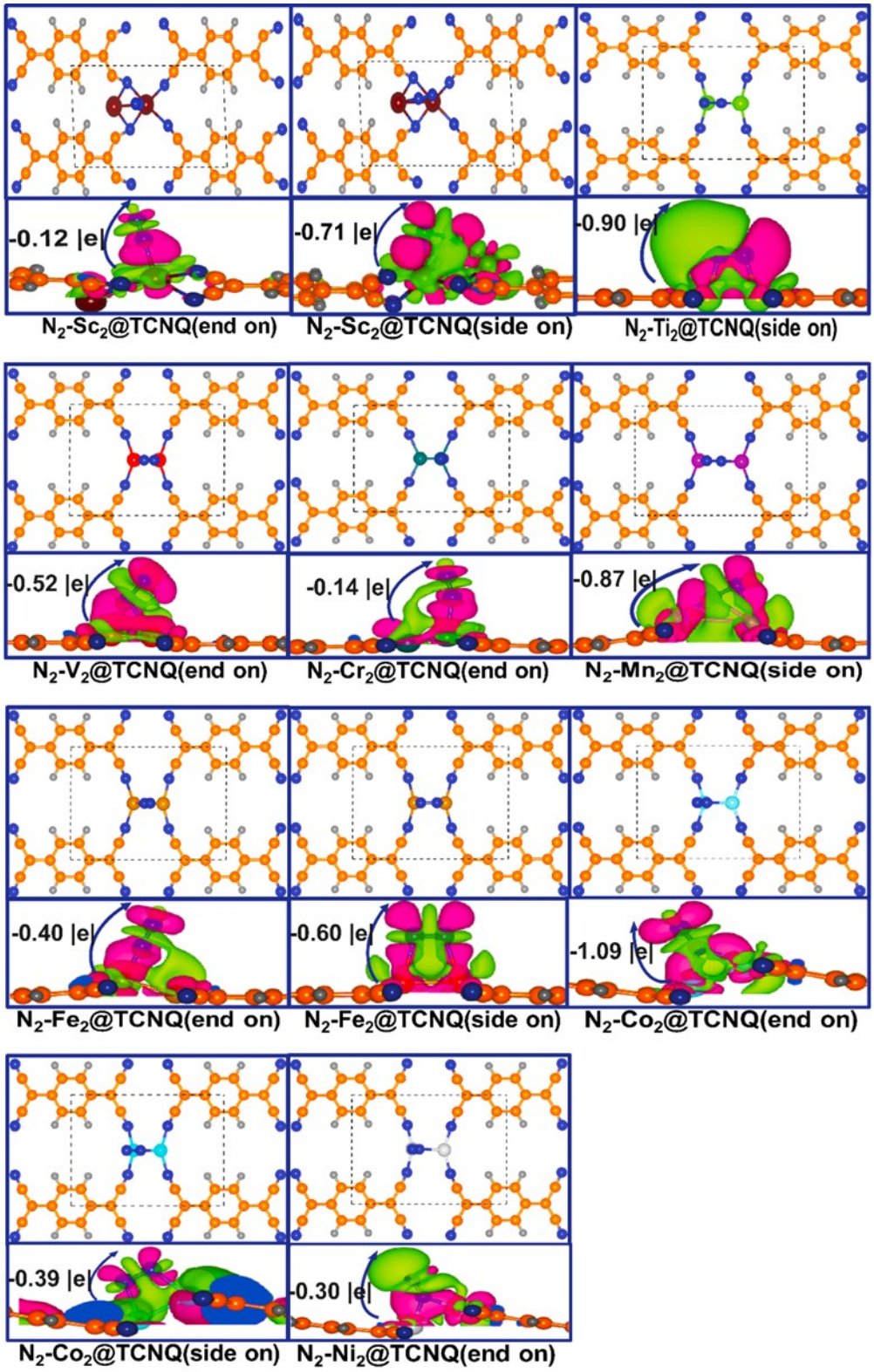
-0.12 |e|
-0.71 |e|
-0.90 |e|
N2-Sc2@TCNQ(end on)
N2-Sc2@TCNQ(side on)
N2-Ti2@TCNQ(side on)
-0.52 |e|
-0.14 |e|
-0.87 |e|
N2-V2@TCNQ(end on)
N2-Cr2@TCNQ(end on)
N2-Mn2@TCNQ(side on)
-0.40 |e|
-0.60 |e|
-1.09 |e|
N2-Fe2@TCNQ(end on)
N2-Fe2@TCNQ(side on)
N2-Co2@TCNQ(end on)
-0.39 |e|
-0.30 |e|
N2-Co2@TCNQ(side on)
N2-Ni2@TCNQ(end on)

(a)

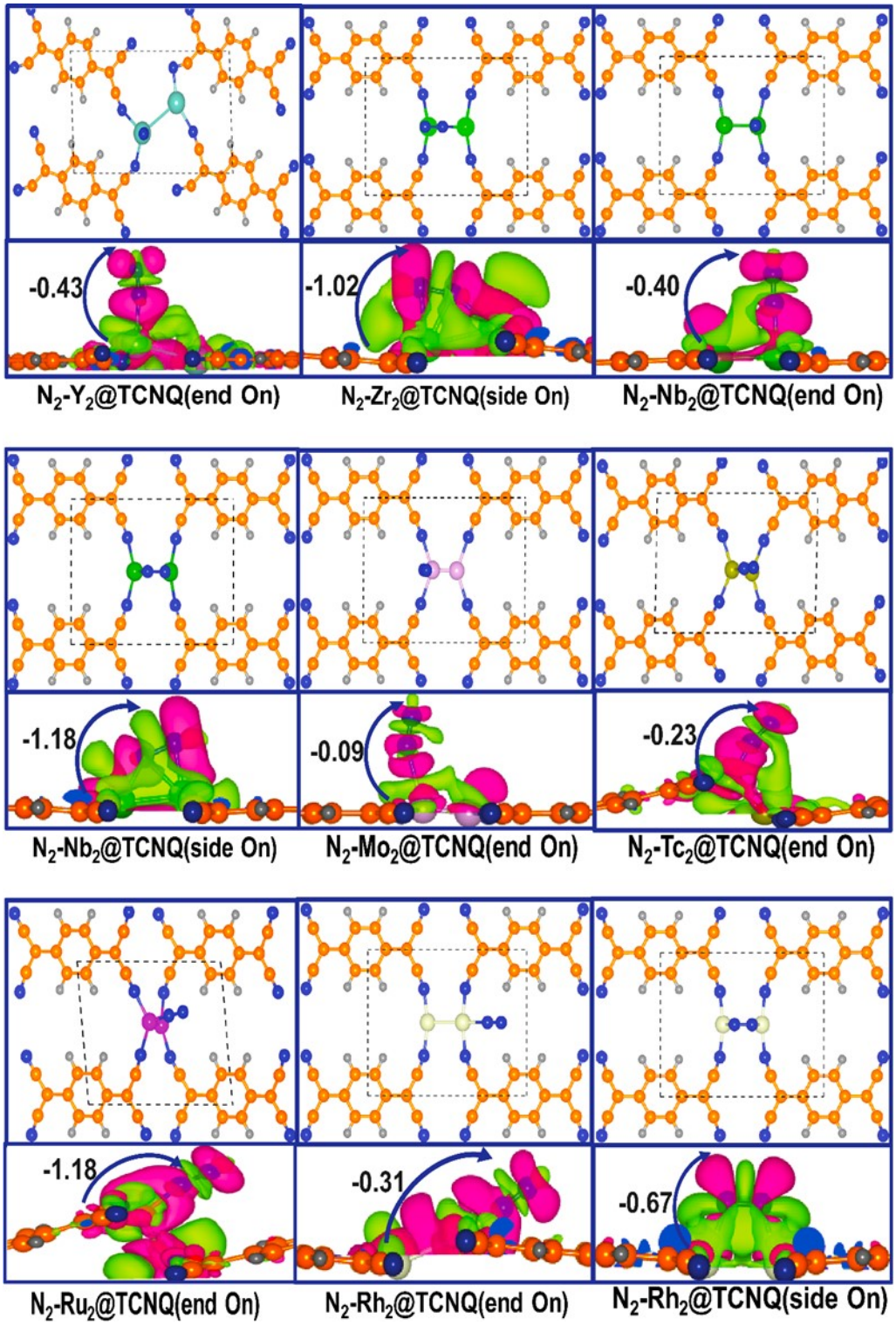
-0.43
-1.02
-0.40
N2-Y2@TCNQ(end On)
N2-Zr2@TCNQ(side On)
N2-Nb2@TCNQ(end On)
-1.18
-0.09
-0.23
N2-Nb2@TCNQ(side On)
N2-Mo2@TCNQ(end On)
N2-Tc2@TCNQ(end On)
-1.18
-0.31
-0.67
N2-Ru2@TCNQ(end On)
N2-Rh2@TCNQ(end On)
N2-Rh2@TCNQ(side On)

(b)

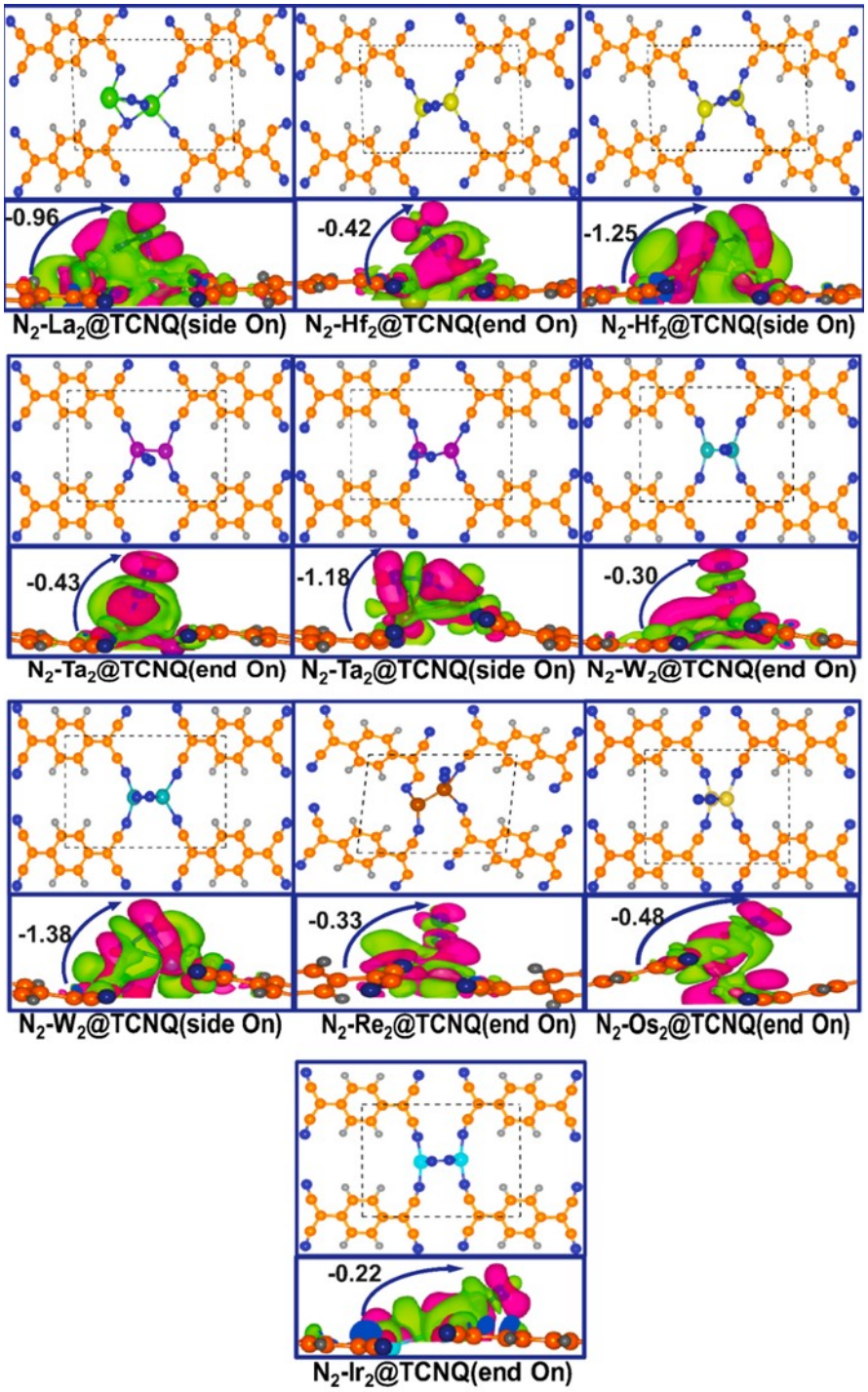

(c)

Fig. S3. Optimized structures (top view) and charge density differences plots of chemisorbed N_2 on (a) 3d, (b) 4d, and (c) 5d DACs. The charge depletion and accumulation are depicted by pink and green colours, respectively. The isosurface value used for plotting the charge density

difference plots is 0.0006 eA^{-3}. The net Bader charge accumulated on the adsorbed N_2 is depicted using blue arrow in the charge density difference plots.

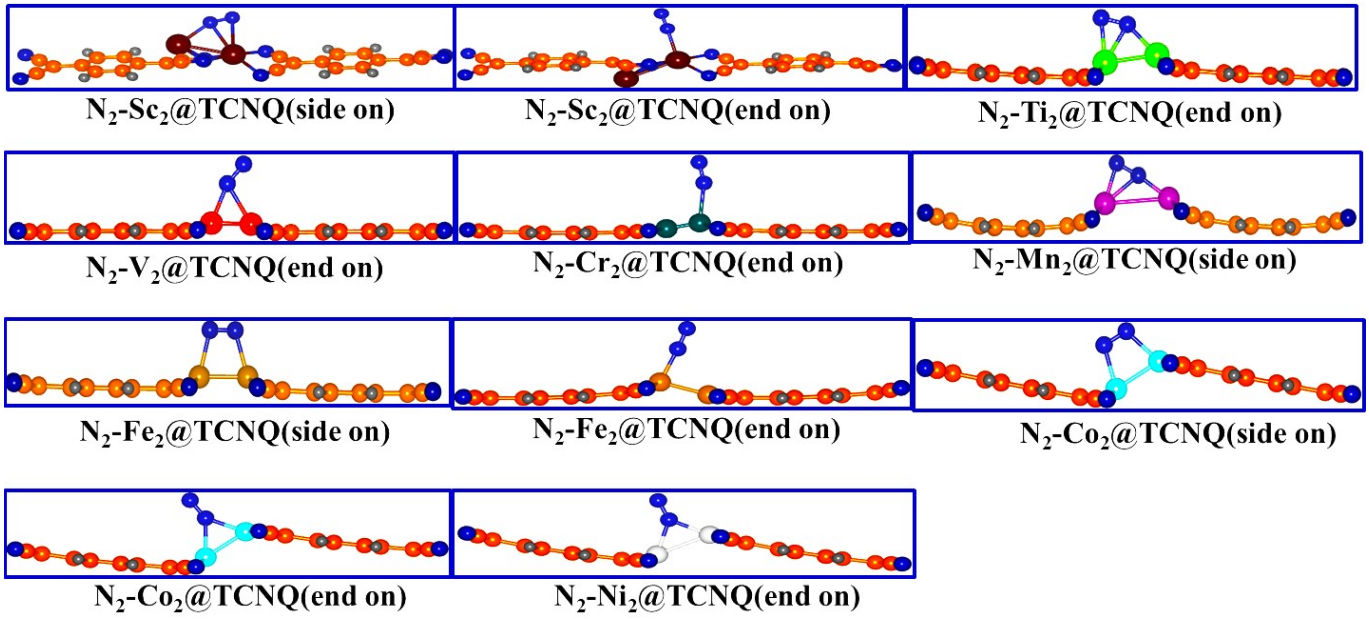

(a)

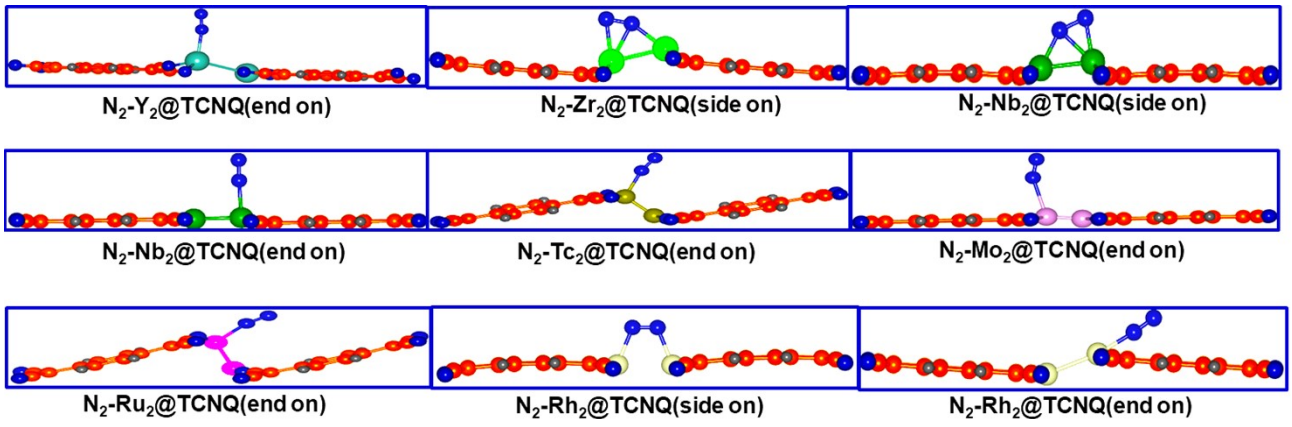

(b)

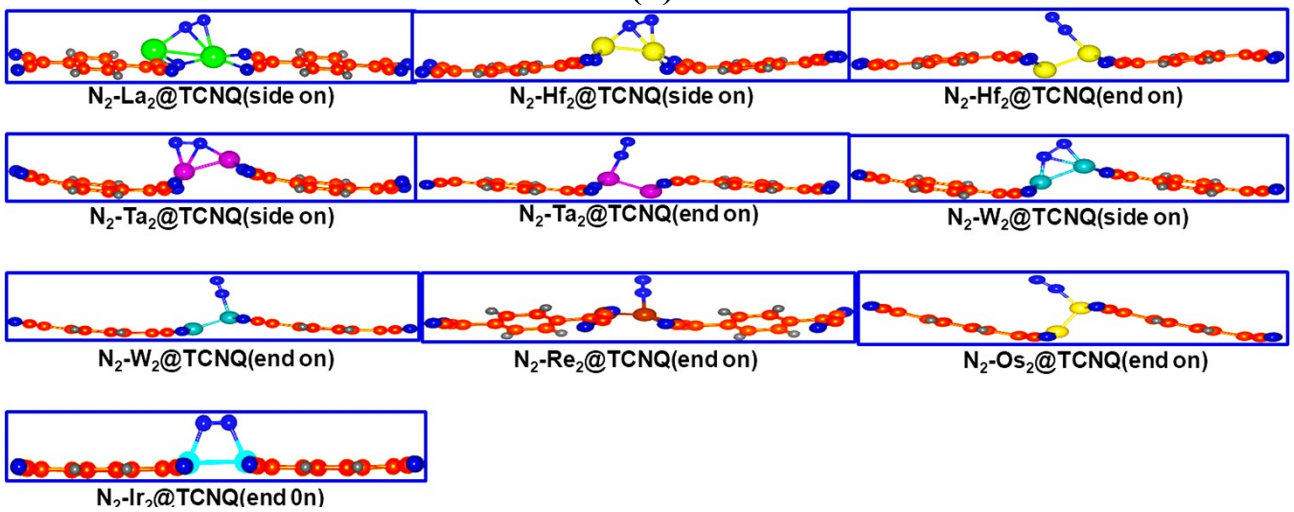

(c)

Fig. S4. Optimized side views of N_2 adsorbed on the active site of (a) 3d, (b) 4d and (c) 5d transition metal-based DACs

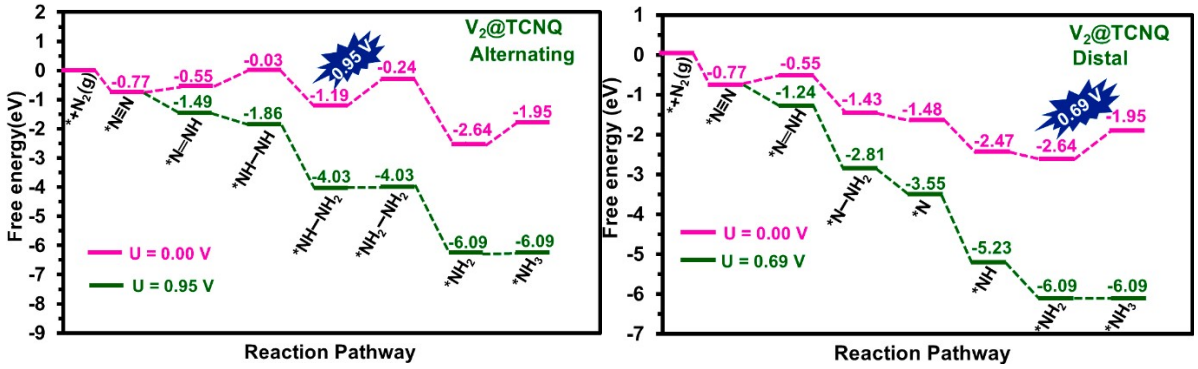

Fig. S5. Free energy profile for NRR on V_2 DAC along alternating and distal mechanisms

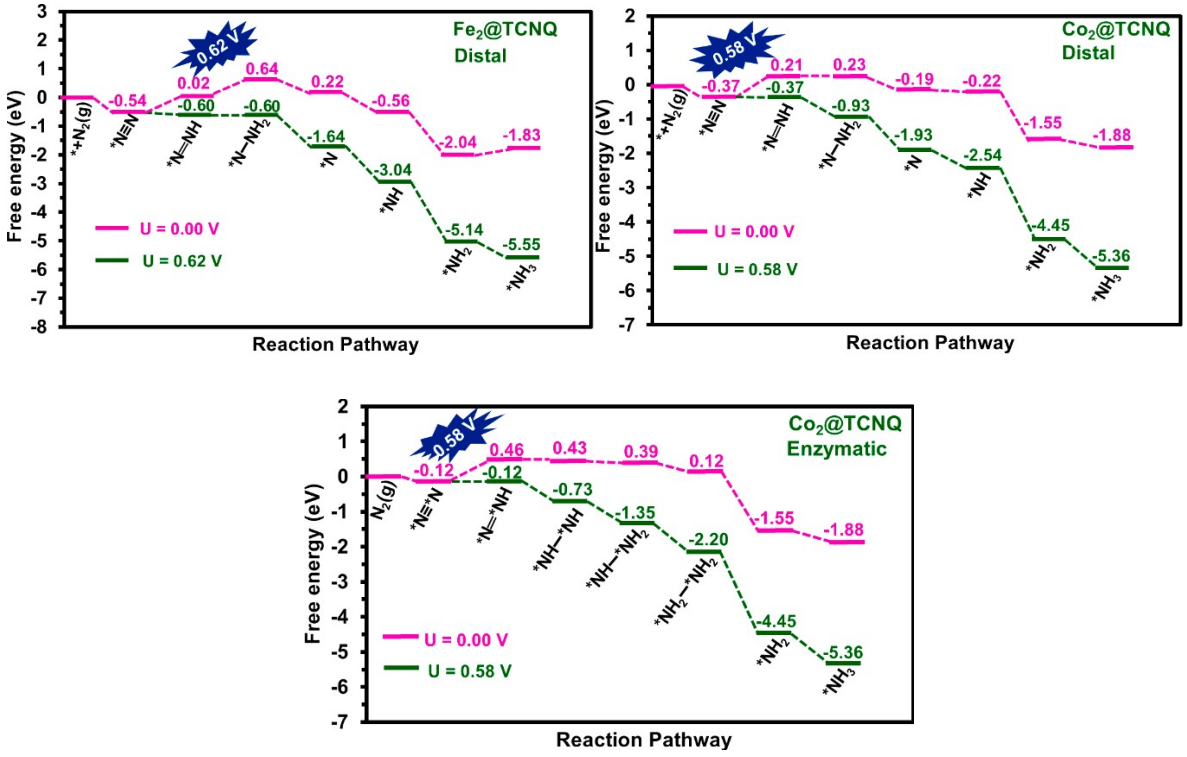

Fig. S6. Free energy profile for NRR on Fe_2 DAC along distal mechanism and on Co_2 DAC along distal and enzymatic mechanisms

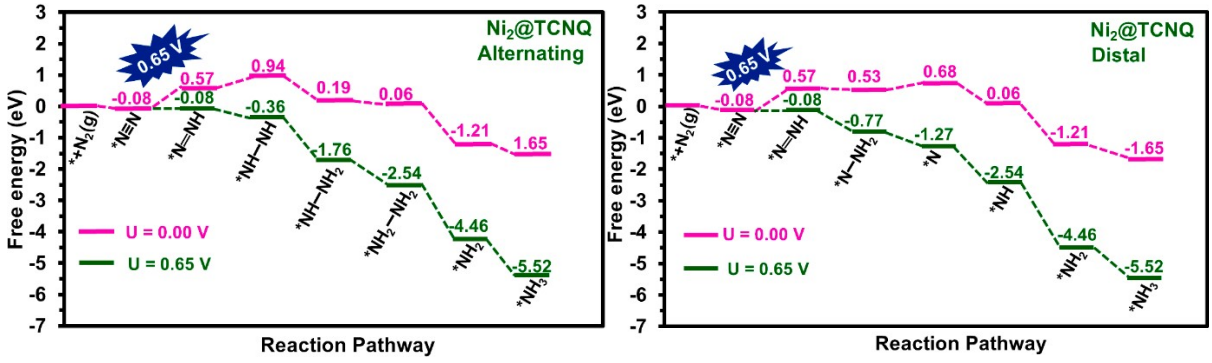

Fig. S7. Free energy profile for NRR on Ni_2 DAC along alternating and distal mechanisms

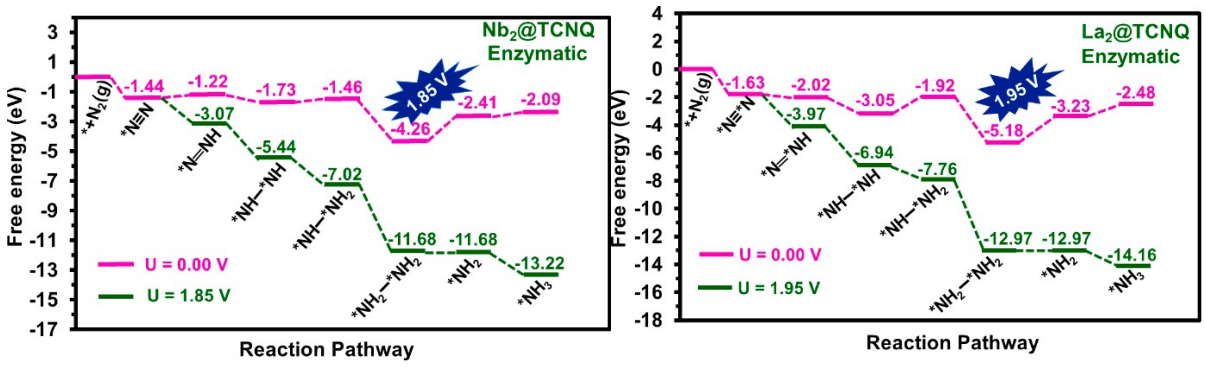

Fig. S8. Free energy profile for NRR on Nb_2 and La_2 DACs along enzymatic mechanism.

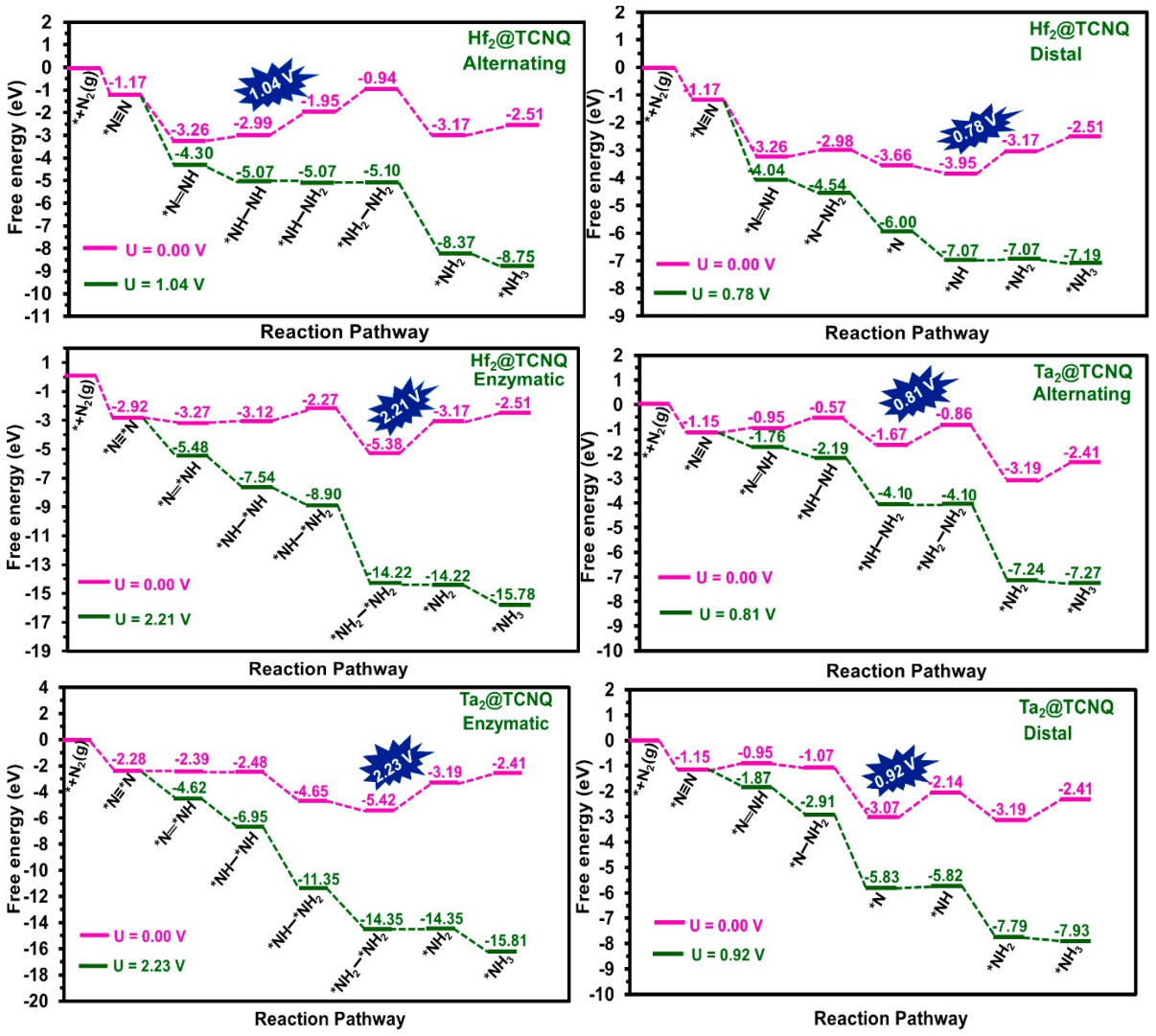

Fig. S9. Free energy profile for NRR on Hf_2 and Ta_2 DACs along alternating, distal and enzymatic mechanisms

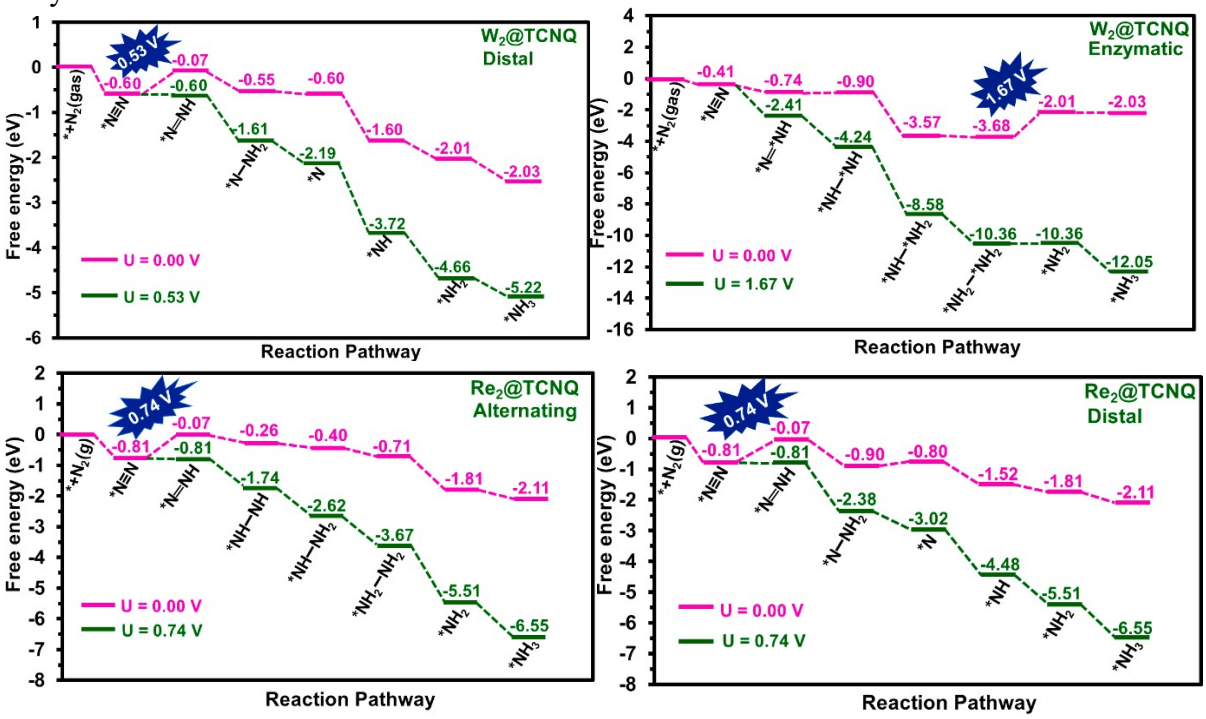

Fig. S10. Free energy profile for NRR on W_2 DAC along distal and enzymatic mechanisms and on Re_2 DAC along alternate and distal mechanisms

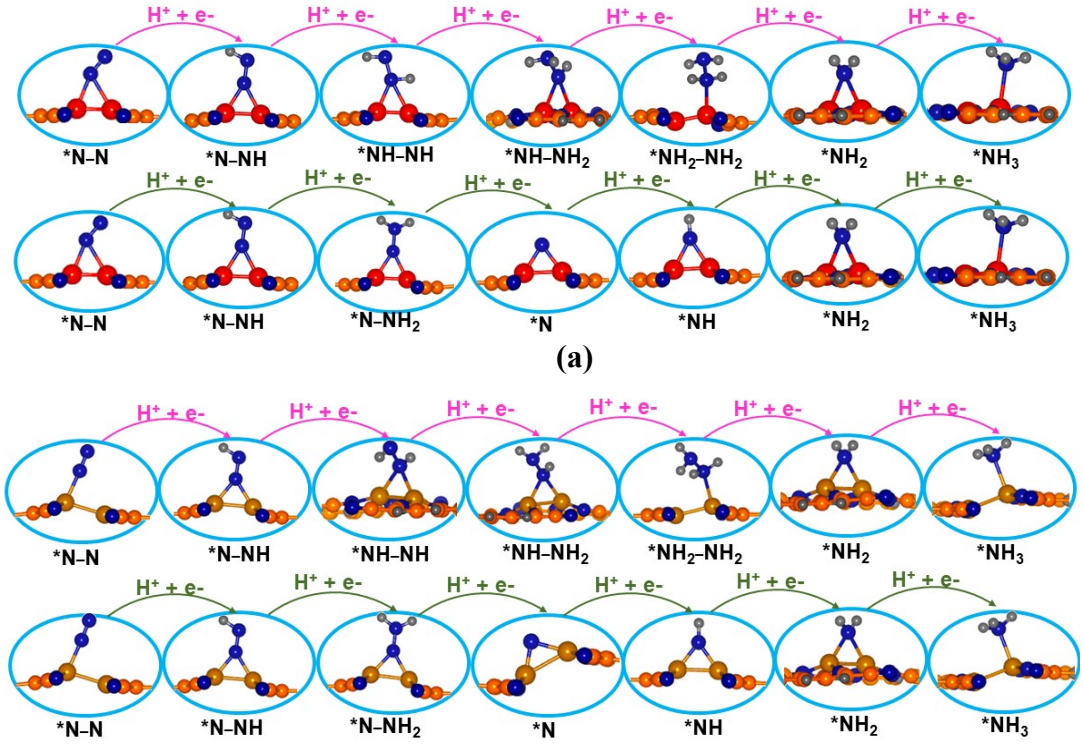

Fig. S11. Optimized truncated side views of NRR intermediates on (a) V_2 and (b) Fe_2 DACs along alternating and distal mechanisms. Pink and green coloured arrows indicate alternating and distal mechanisms respectively

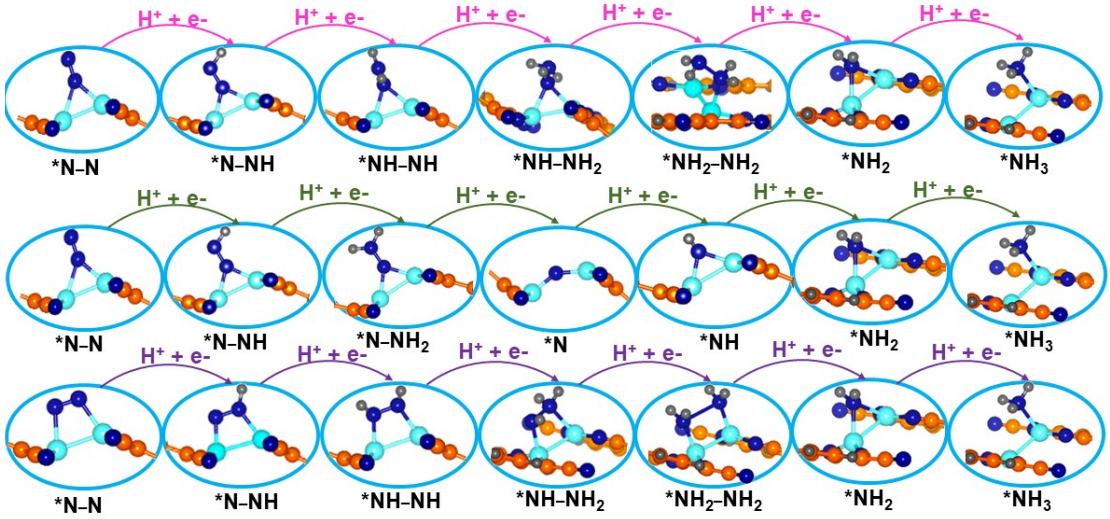

Fig. S12. Optimized truncated side views of NRR intermediates on Co_2 DAC along alternating, distal, and enzymatic mechanisms. Pink, green, and purple-coloured arrows indicate alternating, distal, and enzymatic mechanisms respectively

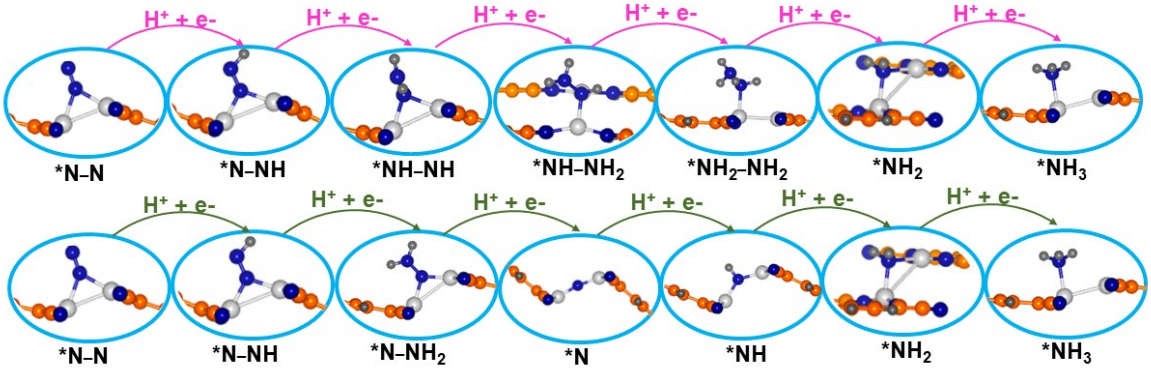

Fig. S13. Optimized truncated side views of NRR intermediates on Ni_2 DAC along alternating and distal mechanisms. Pink and green coloured arrows indicate alternating and distal mechanisms respectively

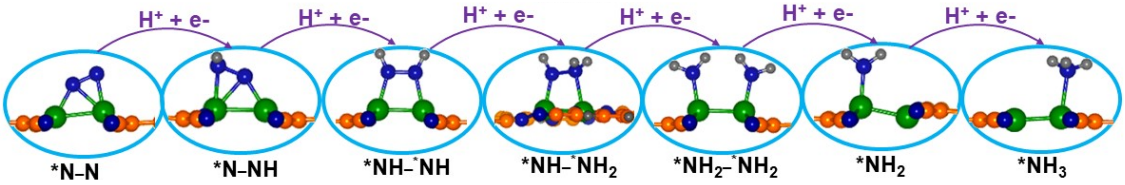

(a)

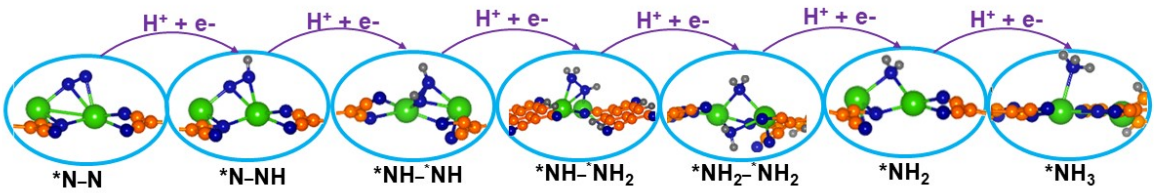

(b)

Fig. S14. Optimized truncated side views of NRR intermediates on (a) Nb_2 and (b) La_2 DACs along enzymatic mechanisms.

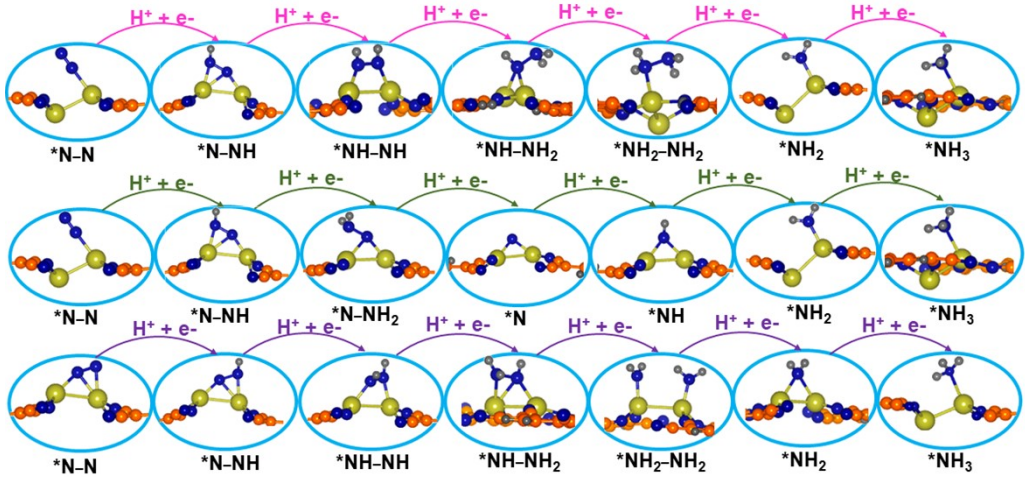

(a)

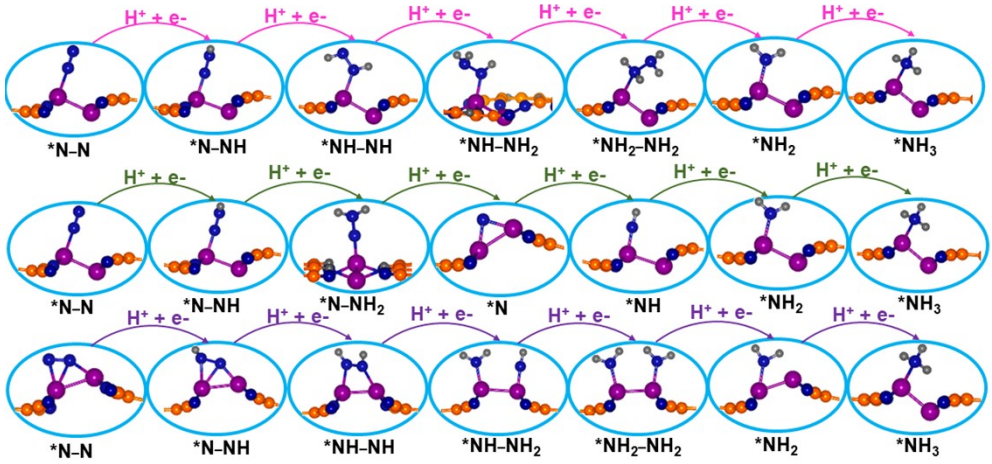

(b)

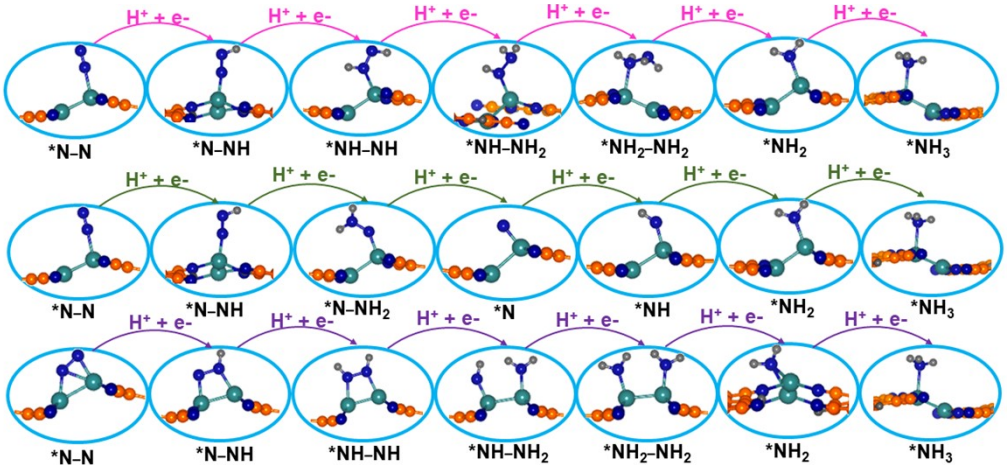

(c)

Fig. S15. Optimized truncated side views of NRR intermediates on (a) Hf_2 (b) Ta_2 and (c) W_2 DACs along alternating, distal, and enzymatic mechanisms. Pink, green, and purple-coloured arrows indicate alternating, distal, and enzymatic mechanisms respectively.

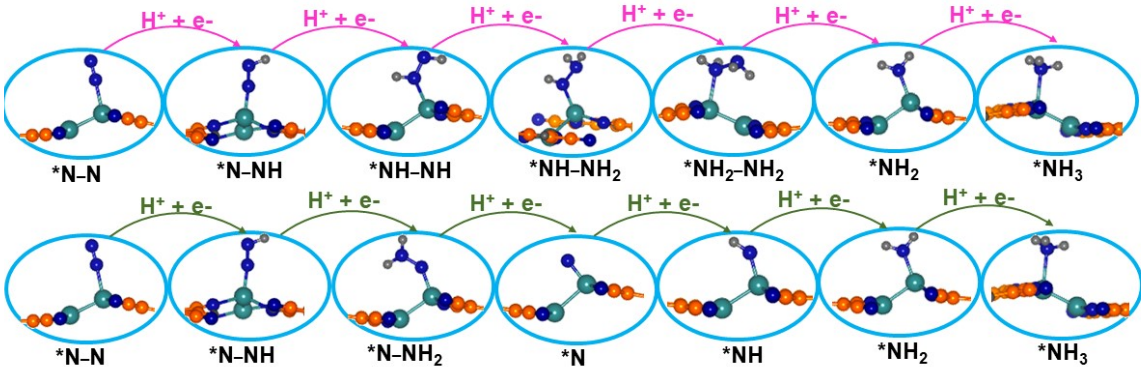

Fig. S16. Optimized truncated side views of NRR intermediates on Re_2 DAC along alternating and distal mechanisms. Pink and green coloured arrows indicate alternating and distal mechanisms respectively.

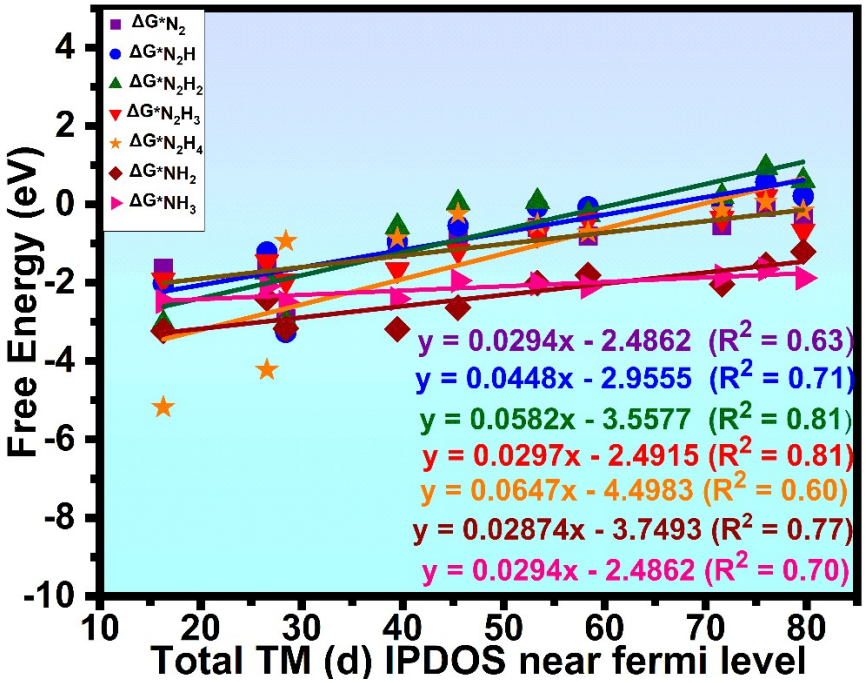

Fig. 17. Free energy changes for adsorption of the NRR intermediates (*N_2, *N_2H, *N_2H_2, *N_2H_3, *N_2H_4, *NH_2 and *NH_3) on the screened DACs: plotted as a function of total transition metal dimer d- states near Fermi level (-3.0 to 3.0 eV). The data points from left to right are for La_2, Nb_2, Hf_2, Ta_2, V_2, W_2, Re_2, Fe_2, Ni_2 and Co_2 catalysts respectively. Solid lines are the fitted linear relation between free energies and total d-states of the intermediates, with the slope and intercept shown in the plot.

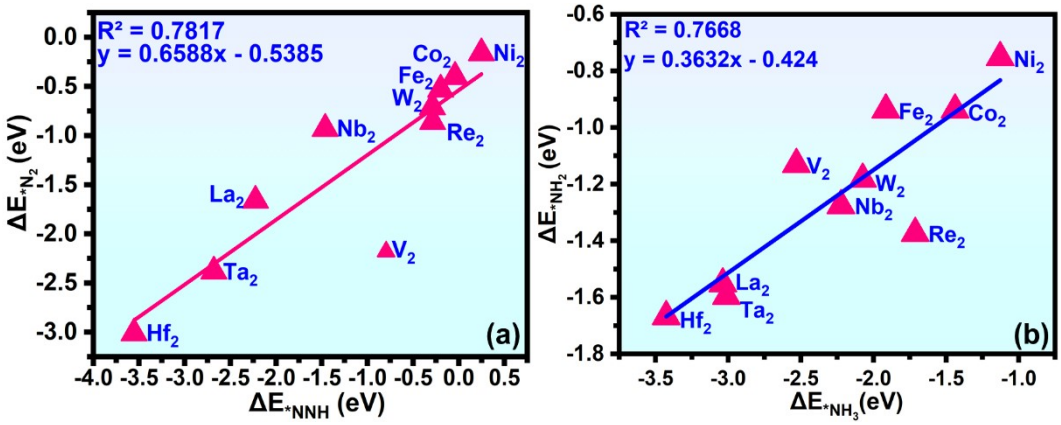

Fig. 18. The correlations between (a) adsorption energies of N_2 (ΔE_{*N_2}) and NNH (ΔE_{*NNH}), (b) adsorption energies of NH_2 (ΔE_{*NH_2}) and NH_3 (ΔE_{*NH_3}) intermediates adsorbed on screened out DACs.

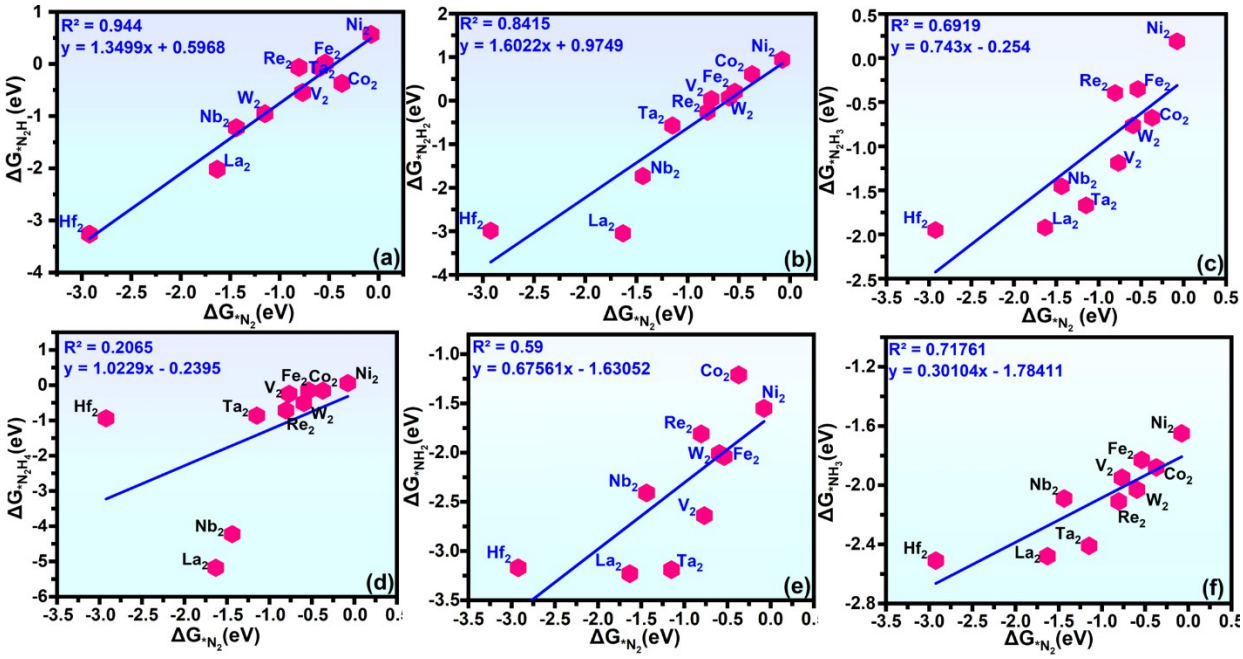

Fig. S19. The scaling relationships for free energy of (a) $*N_2H$ vs $*N_2$, (b)* N_2H_2 vs $*N_2$, (c) $*N_2H_3$ vs $*N_2$, (d) $*N_2H_4$ vs $*N_2$, (e) $*NH_2$ vs $*N_2$, and (f) $*NH_3$ vs $*N_2$ (NRR intermediates on the screened DACs).

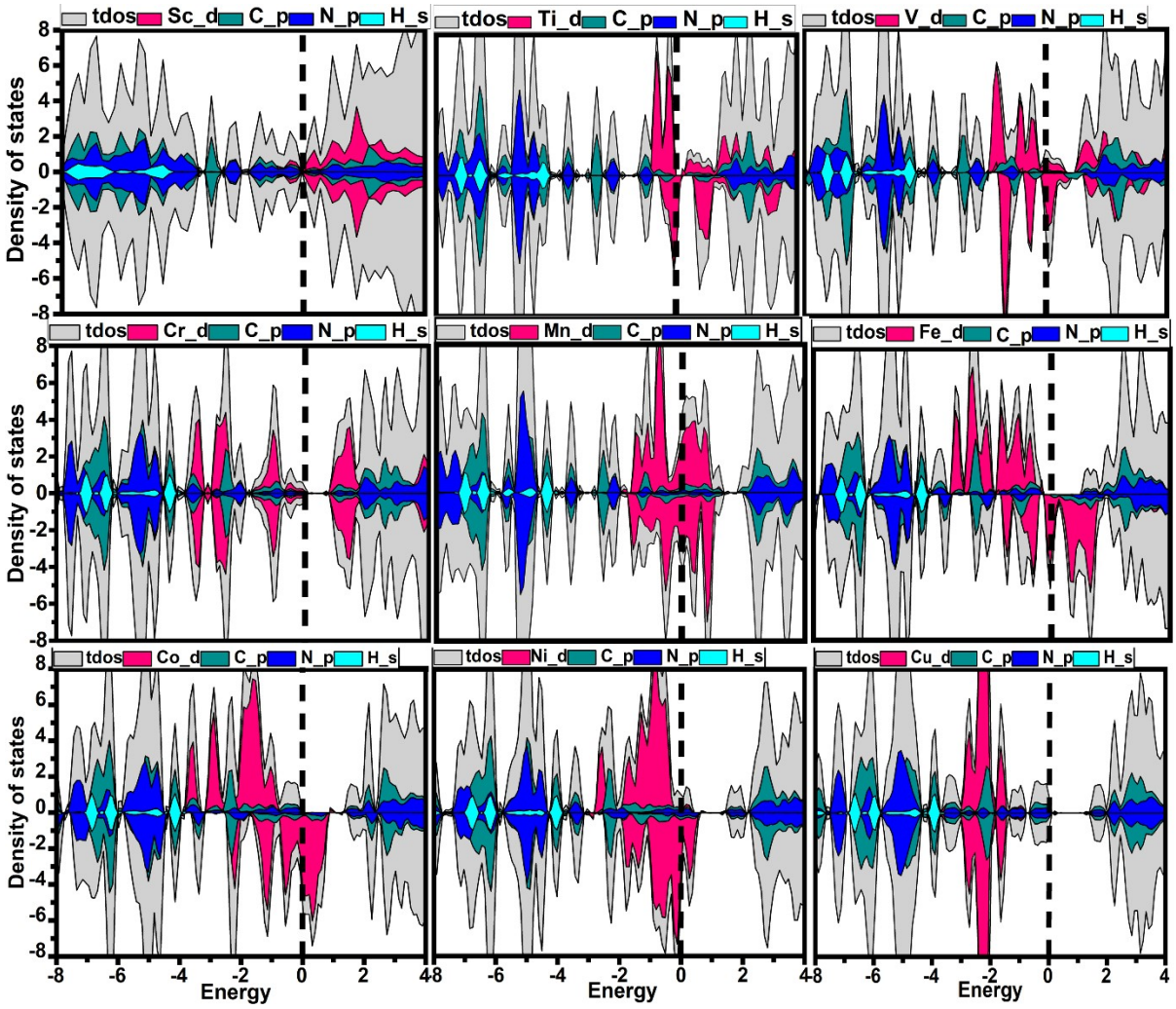
tdos Sc_d C_p N_p H_s
tdos Ti_d C_p N_p H_s
tdos V_d C_p N_p H_s
tdos Cr_d C_p N_p H_s
tdos Mn_d C_p N_p H_s
tdos Fe_d C_p N_p H_s
tdos Co_d C_p N_p H_s
tdos Ni_d C_p N_p H_s
tdos Cu_d C_p N_p H_s
Density of states
Energy

(i)

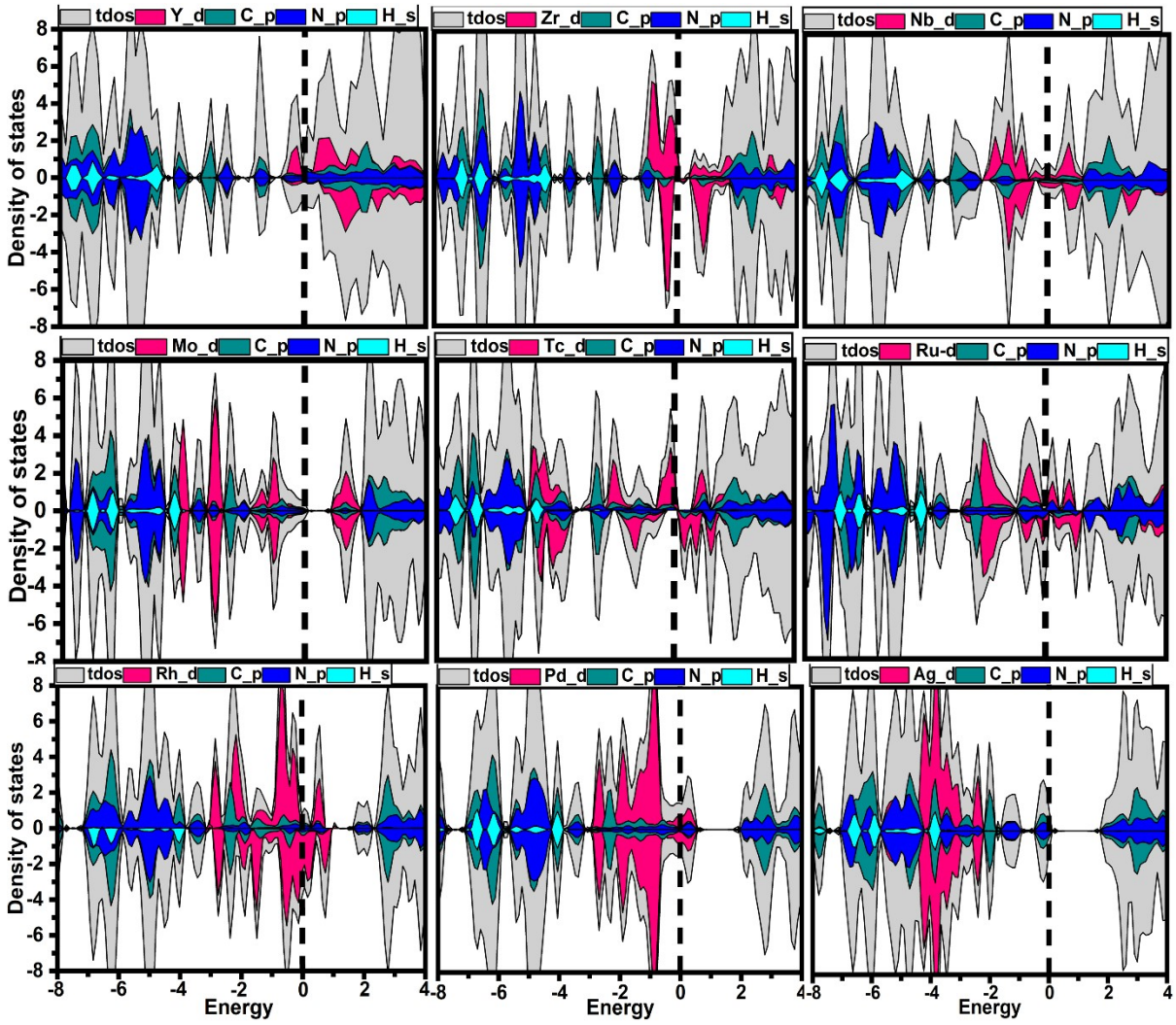
tdos Y_d C_p N_p H_s
tdos Zr_d C_p N_p H_s
tdos Nb_d C_p N_p H_s
tdos Mo_d C_p N_p H_s
tdos Tc_d C_p N_p H_s
tdos Ru-d C_p N_p H_s
tdos Rh_d C_p N_p H_s
tdos Pd_d C_p N_p H_s
tdos Ag_d C_p N_p H_s
Density of states
Energy

(ii)

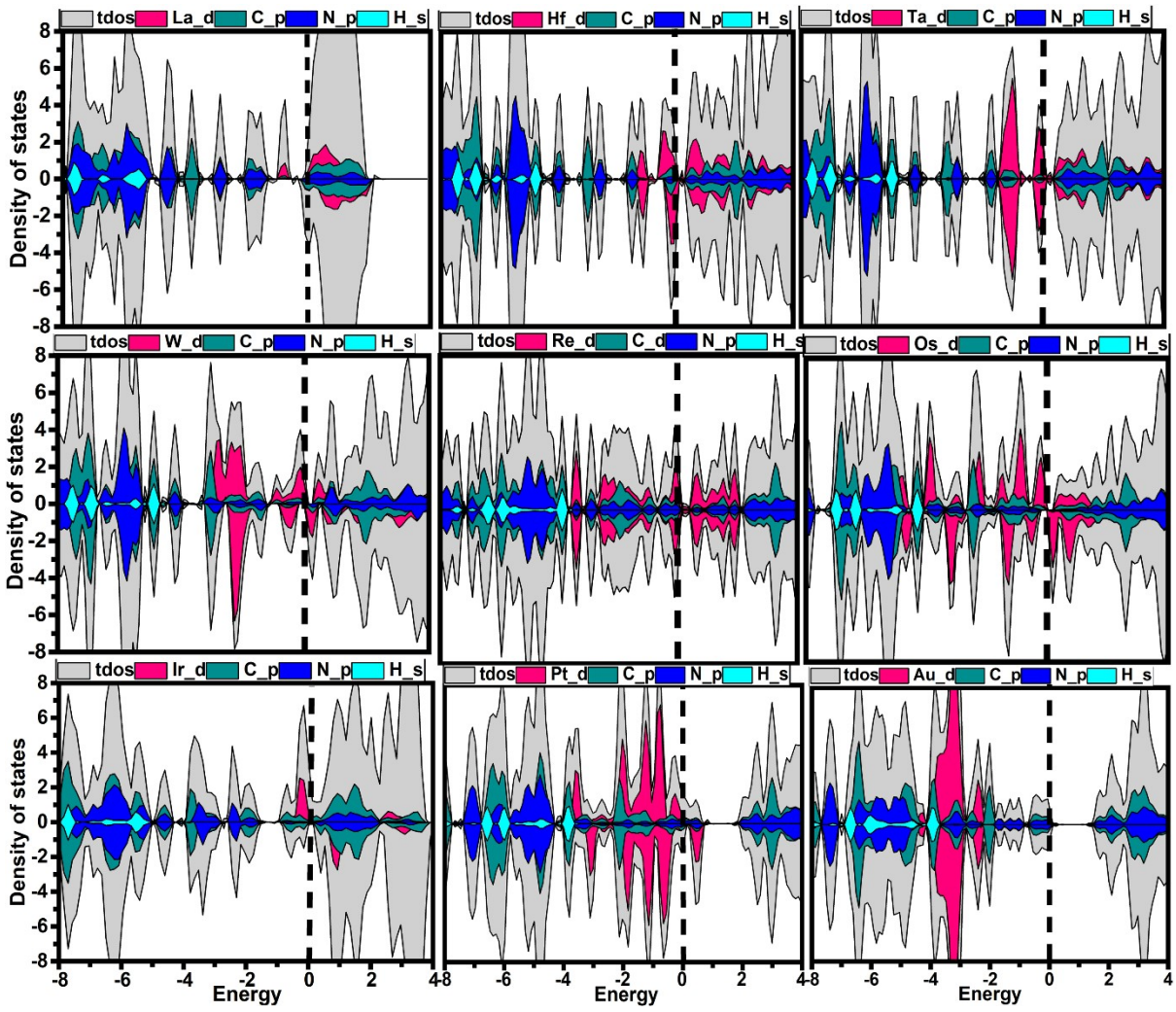

(iii)

Fig. S20. The projected density of states (PDOS) of (i) 3d, (ii) 4d, and (iii)5d transition metal based DACs. The PDOS of the total, TM-d, N-2p, C-2p and H-1s is plotted in grey, pink, dark green, blue and cyan colours, respectively.

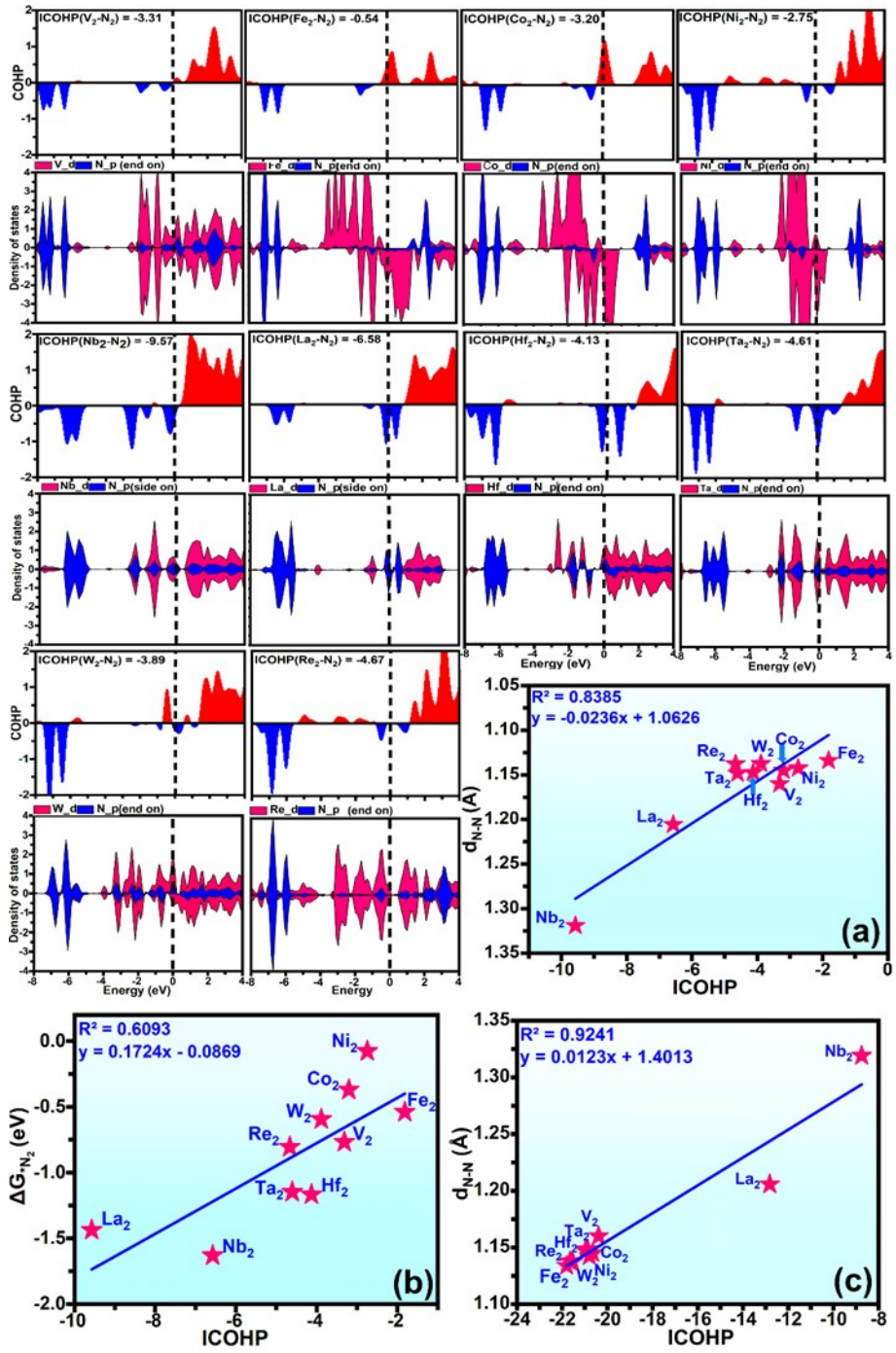

Fig. 21. Computed crystal orbital Hamilton populations (COHPs) and respective orbital projected density of states (oPDOS) for the direct interaction between M_2–N bonds of the N_2 adsorbed on the screened DACs. The bonding and antibonding states in COHP are depicted by blue and red, respectively. Plots representing the correlation between (a) the calculated integrated crystal Hamilton population (ICOHP) of the bond between screened DACs and N atom/atoms of adsorbed $*N_2$ molecule and N-N bond length. (b) the calculated ICOHP of the bond between screened DACs and N atom/atoms of adsorbed $*N_2$ molecule and free energy change for $*N_2$ adsorption (ΔG_{*N_2}) (c) the calculated ICOHP of N-N bond on screened DACs and N-N bond length

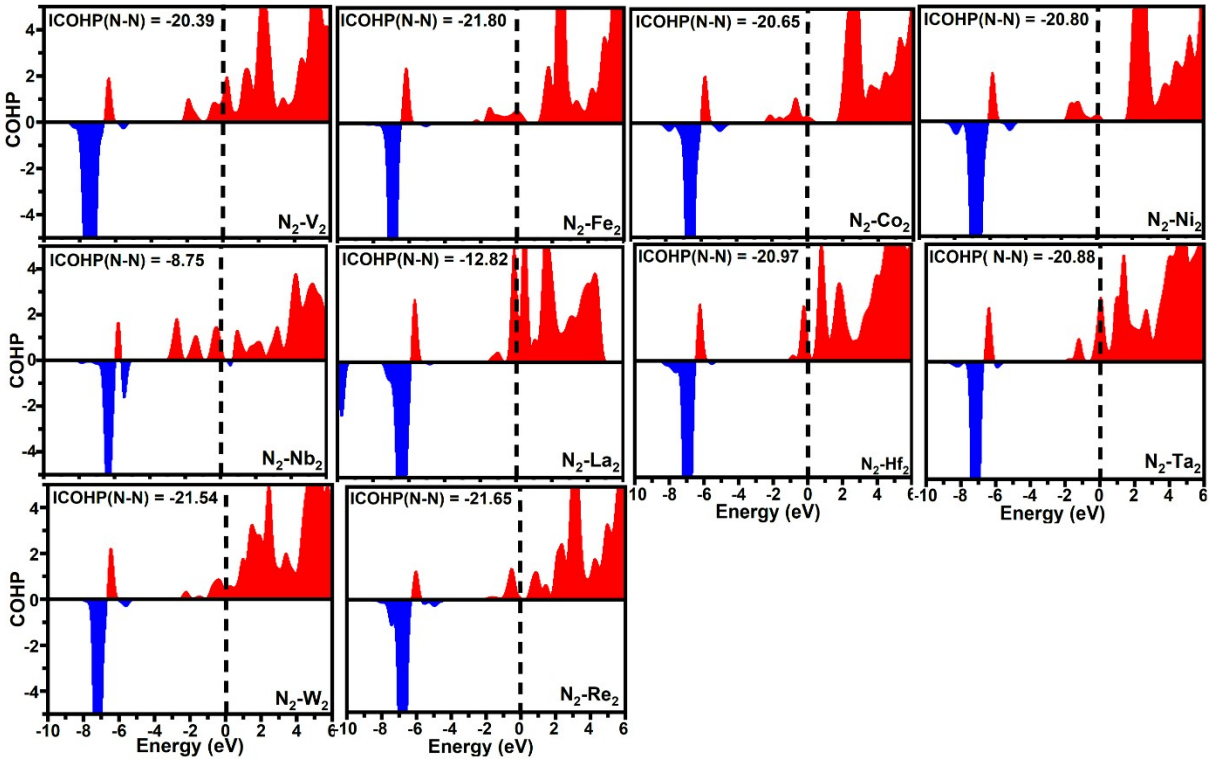

Fig. S22. The crystal orbital Hamilton population (COHP) of N–N bond of N_2 on the screened DACs. The bonding and antibonding states in COHP are depicted by blue and red, respectively.

Table S2. Energy, ZPE, TS, G and ΔG of reaction steps of NRR on V_2, Fe_2 and Ni_2 DACs along alternating and distal mechanisms

Alternating NRR mechanism on V_2

System	Energy	ZPE	TS	G	ΔG
N2P1	-187.98	0.20	0.16	-187.94	-0.77
N2P1-1H	-191.38	0.50	0.14	-191.02	-0.55
N2P1-2H	-194.35	0.79	0.18	-193.74	0.03
N2P1-3H	-199.19	1.05	0.12	-198.26	-1.19
N2P1-4H	-201.87	1.48	0.24	-200.62	-0.25
N1P1-2H	-188.18	0.71	0.08	-187.55	-2.64

N1P1-3H	-191.04	1.01	0.13	-190.17	-1.95

Distal NRR mechanism on V_2

System	Energy	ZPE	TS	G	ΔG
N2P1	-187.98	0.20	0.16	-187.94	-0.77
N2P1-1H	-191.38	0.50	0.14	-191.02	-0.55
N2P1-2H	-195.87	0.83	0.15	-195.20	-1.43
N1P1	-179.84	0.09	0.04	-179.79	-1.48
N1P1-1H	-184.40	0.37	0.06	-184.09	-2.47
N1P1-2H	-188.18	0.71	0.08	-187.55	-2.64
N1P1-3H	-191.04	1.01	0.13	-190.17	-1.95

Alternating NRR mechanism on Fe_2

System	Energy	ZPE	TS	G	ΔG
N2P1	-185.60	0.19	0.18	-185.59	-0.54
N2P1-1H	-188.65	0.48	0.16	-188.33	0.02
N2P1-2H	-192.09	0.81	0.17	-191.44	0.20
N2P1-3H	-196.24	1.13	0.19	-195.30	-0.35
N2P1-4H	-199.64	1.48	0.24	-198.40	-0.15
N1P1-2H	-185.44	0.70	0.09	-184.83	-2.04
N1P1-3H	-188.72	1.01	0.20	-187.92	-1.83

Distal NRR mechanism on Fe_2

System	Energy	ZPE	TS	G	ΔG
N2P1	-185.60	0.19	0.18	-185.59	-0.54
N2P1-1H	-188.65	0.48	0.16	-188.33	0.02
N2P1-2H	-192.30	1.57	0.27	-191.01	0.64
N1P1	-176.00	0.08	0.05	-175.97	0.22
N1P1-1H	-180.31	0.33	0.07	-180.05	-0.56
N1P1-2H	-185.44	0.70	0.09	-184.83	-2.04
N1P1-3H	-188.72	1.01	0.20	-187.92	-1.83

Alternating NRR mechanism on Ni_2

System	Energy	ZPE	TS	G	ΔG
N2P1	-180.29	0.22	0.12	-180.19	-0.08
N2P1-1H	-183.27	0.50	0.07	-182.84	0.57
N2P1-2H	-186.43	0.81	0.15	-185.77	0.94
N2P1-3H	-190.82	1.16	0.16	-189.82	0.19
N2P1-4H	-194.46	1.47	0.27	-193.26	0.06
N1P1-2H	-179.72	0.71	0.07	-179.07	-1.21
N1P1-3H	-183.60	1.01	0.19	-182.77	-1.65

Distal NRR mechanism on Ni_2

System	Energy	ZPE	TS	G	ΔG
N2P1	-180.29	0.22	0.12	-180.19	-0.08
N2P1-1H	-183.27	0.50	0.07	-182.84	0.57
N2P1-2H	-186.84	0.80	.15026760	-186.19	0.53
N1P1	-170.62	0.09	0.05	-170.58	0.67
N1P1-1H	-174.81	0.37	0.06	-174.50	0.06
N1P1-2H	-179.72	0.71	0.07	-179.07	-1.21
N1P1-3H	-183.60	1.01	0.19	-182.77	-1.65

Table S3. Energy, ZPE, TS, G and ΔG of reaction steps of NRR on Co_2 DAC along alternating, distal and enzymatic mechanisms

Alternating NRR mechanism on Co_2

System	Energy	ZPE	TS	G	ΔG
N2P1	-182.87	0.20	0.14	-182.81	-0.37
N2P1-1H	-185.89	0.50	0.14	-185.53	0.21
N2P1-2H	-189.09	0.82	0.16	-188.44	0.61
N2P1-3H	-193.38	0.50	0.14	-193.02	-0.68
N2P1-4H	-197.04	1.49	0.24	-195.80	-0.16
N1P1-2H	-182.36	0.71	0.08	-181.73	-1.55
N1P1-3H	-186.19	1.01	0.19	-185.37	-1.88

Distal NRR mechanism on Co_2

System	Energy	ZPE	TS	G	ΔG
N2P1	-182.87	0.20	0.14	-182.81	-0.37
N2P1-1H	-185.89	0.50	0.14	-185.53	0.21
N2P1-2H	-189.45	0.81	0.17	-188.81	0.23
N1P1	-173.88	0.10	0.00	-173.78	-0.19
N1P1-1H	-177.41	0.36	0.06	-177.11	-0.22
N1P1-2H	-182.36	0.71	0.08	-181.73	-1.54
N1P1-3H	-186.19	1.01	0.19	-185.37	-1.87

Enzymatic NRR mechanism on Co_2

System	Energy	ZPE	TS	G	ΔG
N2P3	-182.65	0.20	0.12	-182.56	-0.12
N2P3-1H	-185.67	0.50	0.11	-185.28	0.46
N2P3-2H	-189.30	0.82	0.13	-188.61	0.43
N2P3-3H	-193.07	1.20	0.08	-191.95	0.39
N2P3-4H	-196.87	1.45	.010	-195.52	0.12
N1P1-2H	-182.36	0.71	0.08	-181.73	-1.54
N1P1-3H	-186.19	1.01	0.19	-185.37	-1.87

Table S4. Energy, ZPE, TS, G and ΔG of reaction steps of NRR on Nb_2 and La_2 DACs along enzymatic mechanisms

Enzymatic NRR mechanism on Nb_2

System	Energy	ZPE	TS	G	ΔG
N2P3	-189.67	0.20	0.08	-189.55	-1.44
N2P3-1H	-192.98	0.48	0.13	-192.63	-1.22
N2P3-2H	-197.12	0.81	0.13	-196.44	-1.73
N2P3-3H	-200.46	1.15	0.15	-199.47	-1.46
N2P3-4H	-206.65	1.34	0.22	-205.54	-4.23
N1P1-2H	-188.81	0.67	0.12	-188.26	-2.41
N1P1-3H	-192.12	1.01	0.13	-191.25	-2.09

Enzymatic NRR mechanism on La_2

System	Energy	ZPE	TS	G	ΔG
N2P3	-184.63	0.18	0.13	-184.58	-1.63
N2P3-1H	-188.58	0.46	0.14	-188.27	-2.02
N2P3-2H	-193.25	0.78	0.13	-192.59	-3.05
N2P3-3H	-195.69	1.12	0.20	-194.77	-1.92
N2P3-4H	-202.43	1.32	0.22	-201.33	-5.18
N1P1-2H	-184.46	0.65	0.11	-183.93	-3.23
N1P1-3H	-187.24	0.98	0.21	-186.47	-2.48

Table S5. Energy, ZPE, TS, G and ΔG of reaction steps of NRR on Hf_2, Ta_2 and W_2 DACs along alternating, distal and enzymatic mechanisms

Alternating NRR mechanism on Hf_2

System	Energy	ZPE	TS	G	ΔG
N2P1	-189.16	0.38	0.21	-188.99	-1.17
N2P1-1H	-194.78	0.48	0.08	-194.38	-3.26
N2P1-2H	-198.06	0.80	0.14	-197.40	-2.99
N2P1-3H	-200.61	1.13	0.19	-199.67	-1.95
N2P1-4H	-203.23	1.49	0.22	-201.96	-0.94
N1P1-2H	-189.23	0.64	0.14	-188.73	-3.17
N1P1-3H	-192.22	1.01	0.16	-191.38	-2.51

Distal NRR mechanism on Hf_2

System	Energy	ZPE	TS	G	ΔG
N2P1	-189.16	0.38	0.21	-188.99	-1.17
N2P1-1H	-194.78	0.48	0.08	-194.38	-3.26
N2P1-2H	-198.15	0.87	0.12	-197.40	-2.98
N1P1	-182.66	0.09	0.05	-182.63	-3.66

N1P1-1H	-186.52	0.35	0.04	-186.21	-3.95
N1P1-2H	-189.23	0.64	0.14	-188.73	-3.17
N1P1-3H	-192.22	1.01	0.16	-191.38	-2.51

Enzymatic NRR mechanism on Hf_2

System	Energy	ZPE	TS	G	ΔG
N2P3	-190.86	0.20	0.09	-190.74	-2.92
N2P3-1H	-194.78	0.48	0.08	-194.39	-3.27
N2P3-2H	-198.22	0.81	0.13	-197.54	-3.12
N2P3-3H	-201.02	1.13	0.11	-199.99	-2.27
N2P3-4H	-207.38	1.28	0.30	-206.39	-5.38
N1P1-2H	-189.23	0.64	0.14	-188.73	-3.17
N1P1-3H	-192.22	1.01	0.16	-191.38	-2.51

Alternating NRR mechanism on Ta_2

System	Energy	ZPE	TS	G	ΔG
N2P1	-191.25	0.20	0.10	-191.15	-1.15
N2P1-1H	-194.58	0.49	0.17	-194.26	-0.95
N2P1-2H	-197.77	0.80	0.21	-197.18	-0.57
N2P1-3H	-202.48	1.13	0.22	-201.58	-1.67
N2P1-4H	-205.35	1.49	0.21	-204.07	-0.86
N1P1-2H	-191.50	0.67	0.11	-190.4	-3.19
N1P1-3H	-194.34	1.02	0.14	-193.46	-2.41

Distal NRR mechanism on Ta_2

System	Energy	ZPE	TS	G	ΔG
N2P1	-191.25	0.20	0.10	-191.15	-1.15
N2P1-1H	-194.58	0.49	0.17	-194.26	-0.95
N2P1-2H	-198.34	0.80	0.13	-197.67	-1.07
N1P1	-184.28	0.09	0.04	-184.22	-3.07
N1P1-1H	-186.85	0.35	0.10	-186.59	-2.14
N1P1-2H	-191.50	0.67	0.11	-190.4	-3.19
N1P1-3H	-194.34	1.02	0.14	-193.46	-2.41

Enzymatic NRR mechanism on Ta_2

System	Energy	ZPE	TS	G	ΔG
N2P1	-192.42	0.21	0.07	-192.28	-2.28
N2P1-1H	-196.10	0.50	0.10	-195.70	-2.39
N2P1-2H	-199.73	0.79	0.14	-199.08	-2.48
N2P1-3H	-205.36	1.01	0.21	-204.56	-4.65
N2P1-4H	-209.73	1.33	0.23	-208.63	-5.42
N1P1-2H	-191.50	0.67	0.11	-190.4	-3.19
N1P1-3H	-194.34	1.02	0.14	-193.46	-2.41

Alternating NRR mechanism on W_2

System	Energy	ZPE	TS	G	ΔG
N2P1	-192.25	0.23	0.09	-192.11	-0.60
N2P1-1H	-195.21	0.49	0.16	-194.89	-0.07
N2P1-2H	-198.69	0.82	0.18	-198.05	0.07
N2P1-3H	-203.07	1.05	0.16	-202.18	-0.77
N2P1-4H	-206.49	1.49	0.23	-205.22	-0.51
N1P1-2H	-191.94	0.73	0.07	-191.27	-2.01
N1P1-3H	-195.44	1.02	0.18	-194.60	-2.03

Distal NRR mechanism on W_2

System	Energy	ZPE	TS	G	ΔG
N2P1	-192.25	0.23	0.09	-192.11	-0.60
N2P1-1H	-195.21	0.49	0.16	-194.89	-0.07
N2P1-2H	-199.30	0.81	0.18	-198.67	-0.55
N1P1	-183.28	0.08	0.06	-183.26	-0.60
N1P1-1H	-187.84	0.36	0.08	-187.56	-1.60
N1P1-2H	-191.94	0.73	0.07	-191.27	-2.01
N1P1-3H	-195.44	1.02	0.18	-194.60	-2.03

Enzymatic NRR mechanism on W_2

System	Energy	ZPE	TS	G	ΔG
N2P1	-192.03	0.19	0.08	-191.93	-0.41
N2P1-1H	-195.95	0.50	0.11	-195.56	-0.74
N2P1-2H	-199.68	0.80	0.14	-199.02	-0.90
N2P1-3H	-205.87	1.05	0.16	-204.98	-3.57
N2P1-4H	-209.57	1.36	0.19	-208.40	-3.68
N1P1-2H	-191.94	0.73	0.07	-191.27	-2.01
N1P1-3H	-195.44	1.02	0.18	-194.60	-2.03

Table S6. Energy, ZPE, TS, G and ΔG of reaction steps of NRR on Re_2 DAC along alternating and distal mechanisms

Alternating NRR mechanism on Re_2

System	Energy	ZPE	TS	G	ΔG
N2P1	-190.81	0.22	0.14	-190.73	-0.81
N2P1-1H	-193.62	0.49	0.16	-193.29	-0.07
N2P1-2H	-197.47	0.85	0.15	-196.78	-0.26
N2P1-3H	-201.24	1.13	0.11	-200.22	-0.40
N2P-4H	-205.17	1.51	0.19	-203.84	-0.71
N1P1-2H	-190.12	0.69	0.06	-189.48	-1.81
N1P1-3H	-194.04	1.04	0.09	-193.08	-2.11

Distal NRR mechanism on Re_2

System	Energy	ZPE	TS	G	ΔG
N2P1	-190.81	0.22	0.14	-190.73	-0.81
N2P1-1H	-193.62	0.49	0.16	-193.29	-0.07
N2P1-2H	-198.14	0.82	0.10	-197.42	-0.90
N1P1	-181.90	0.09	0.06	-181.87	-0.80
N1P1-1H	-186.20	0.38	0.07	-185.89	-1.52
N1P1-2H	-190.12	0.69	0.06	-189.48	-1.81
N1P1-3H	-194.04	1.04	0.09	-193.08	-2.11